c.3

The Effects of Cosolidifying MAN/AN and

QMAN/AN on the Performance of a Nonideal Explosive

by

B. G. Craig
J. Hershkowitz*
A. W. Campbell
Ray Engelke

*Explosives Division, Feltman Research Laboratory,
Picatinny Arsenal, Dover, NJ 07801.

los alamos
scientific laboratory
of the University of California
LOS ALAMOS, NEW MEXICO 87545

An Affirmative Action/Equal Opportunity Employer

The citation in this report of the names of commercial firms or of commercially available products or services does not constitute offical endorsement or approval of such commercial firms, products, or services by the US government.

THE EFFECTS OF COSOLIDIFYING MAN/AN AND

QMAN/AN ON THE PERFORMANCE OF A NONIDEAL EXPLOSIVE

by

B. G. Craig, J. Hershkowitz, A. W. Campbell, and Ray Engelke

ABSTRACT

It is shown that performance of 40 RDX/60 (MAN + AN) and
40 RDX/60 (QMAN + AN) improves as the MAN or QMAN is increased
to the CO balance. Both small-scale and large-scale tests were
conducted with the formulation containing MAN. The data are
interpreted by a variety of methods. It is concluded that an
intimate mix of MAN with AN results in a greater energy release
per unit volume of AN than occurs when the MAN is not present.
New methods for evaluating cylinder test data are proposed.

I.   INTRODUCTION

"Ideal" explosives are those whose detonation
properties are not dependent in a major way on the
charge size for sizes large compared to the minimum
that will propagate a detonation. PETN, HMX, RDX,
TNT, and mixtures of these are examples of ideal ex-
plosives. Nonideal explosives are those whose deto-
nation properties are strongly dependent on the
charge size. Nonideal explosives are usually com-
posite explosives; i.e., explosives that are a mix-
ture of particulate oxidizers and/or fuels. Non-
ideal explosives may contain an ideal explosive as
an ingredient. ANFO (ammonium nitrate/fuel oil),
60/40 Amatol (60 wt% ammonium nitrate/40 wt% TNT),
and Amatex 20 (20 wt% RDX/40 wt% TNT/40 wt% ammonium
nitrate) are examples of nonideal explosives.

There are potential advantages for the use of
composite explosives in many applications. These
advantages result from the relatively low cost and
availability of particulate oxidizers and/or fuels
and from the fact that these ingredients are not ex-
plosives until they have been mixed. The main dis-

advantage of current composite explosives is that
they do not fully react on the time scale needed for
many applications--especially that of fragmentation
munitions.

Historically, the ideality of an explosive was
first determined by measuring the detonation velo-
city as a function of the charge diameter.[1] More
recently, measurement of relative energy by means of
the cylinder test[2 - 4] has been combined with calcu-
lations[5 - 7] to obtain a more quantitative measure
of the mass fraction that fails to react fully on a
time scale of interest. Most recently, Hershkowitz
and Akst[7] have combined measurements of detonation
velocity and plate dent in very small, but heavily
confined, geometry with calculations. More impor-
tantly, their work exemplified a new approach to the
problem of overcoming the slow reaction of composite
explosives, i.e. by obtaining an intimate mix by
cosolidification of the fuel and oxidizer. Previous
efforts to improve intimacy of mixing in nonideal
explosives had been limited to use of smaller par-
ticulates prior to combining fuel and oxidizer.[5,8]
This report extends the work of Hershkowitz and Akst.

1

Experiments are described in which mono- and tetra-methyl ammonium nitrate (MAN and QMAN,respectively) were systematically substituted for ammonium nitrate (AN) in 40 wt% RDX/60 wt% AN. MAN is an explosive whereas QMAN is not. An apparent synergistic effect was observed, as evidenced by an enhancement of plate-dent depth in small-scale experiments, for each substitute fuel (MAN and QMAN). Detonation velocities and cylinder wall velocities were mea-sured in large scale (100-mm diam) for selected for-mulations with MAN to determine if the apparent syn-ergistic effect is general or an artifact of small geometry. The detonation velocity data comparisons with BKW calculations, in which the fraction of AN that reacts was varied for a given formulation, show that the equivalent of about 50% of AN reacts on a short enough time scale to affect detonation velo-city. The cylinder-wall velocity data show that sub-stitution of 15 or more percent MAN for AN results in greater acceleration of the wall at late times, which suggests the equivalent of additional AN re-action within the time scale of the cylinder test. Accordingly, some fraction of the synergism observed at small dimensions has extended to far larger di-mensions.

II. DESCRIPTION OF EXPERIMENTS

Hershkowitz and Akst studied the effects of substituting MAN and QMAN for AN in the explosives Amatex 20 (20 wt% RDX/40 wt% TNT/40 wt% AN) and Ama-tol (60 wt% TNT/40 wt% AN). Their experiments were limited to small scale (similar to the small-scale experiments described below). Since MAN and QMAN improved the small-scale performance of Amatex/20 and Amatol, presumably by increasing the early re-action of AN, the explosive chosen for the current study consisted of 40 wt% RDX and 60 wt% (MAN + AN or QMAN + AN). TNT was omitted because it had been found to be incompatible with MAN and QMAN. A major objective of this study was to obtain data from large-scale as well as small-scale experiments; ac-cordingly, cylinder tests at 100-mm-explosive diame-ter were scheduled.

Those compositions containing MAN or QMAN are potentially castable; however, all charges used for this study were prepared instead by pressing blends of RDX with ground, solidified melts of the poten-tially synergistic components AN + MAN or AN + QMAN. This choice circumvented the need for a casting

study, and allowed for a more direct comparison with pure RDX. It also reduced the likelihood that small-scale screening tests would fall below the failure diameter, since in general, pressed charges propa-gate in smaller diameters than cast charges. The procedure used to prepare charges is given in Appen-dix A. Results of safety and physical studies are given in Appendix B.

The explosive compositions were screened for performance by means of small-scale rate (detonation velocity) and plate-dent tests. Pellets of the var-ious compositions were pressed to a nominal diameter of 9.53 mm (0.375 in.) and machined to a uniform length. In general, two charges (seven pellets each) were prepared for each composition. An effort was made to assemble the pellets into two similar char-ges on the basis of density, and to assemble the pel-lets in any one charge to give a nearly constant den-sity over the last five or six pellets.

Charges were assembled in brass tubes with ion-ization switches (to measure detonation velocity) and a witness plate (to measure dent) as shown in Figs. 1 and 2. The clearance between the brass and the pellets ranged between 0.025 and 0.051 mm. Assembly was accomplished by pushing a pellet through the tube
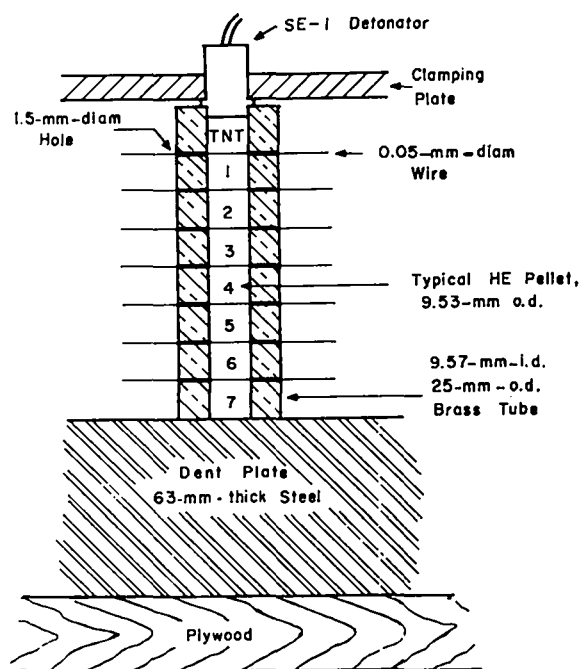

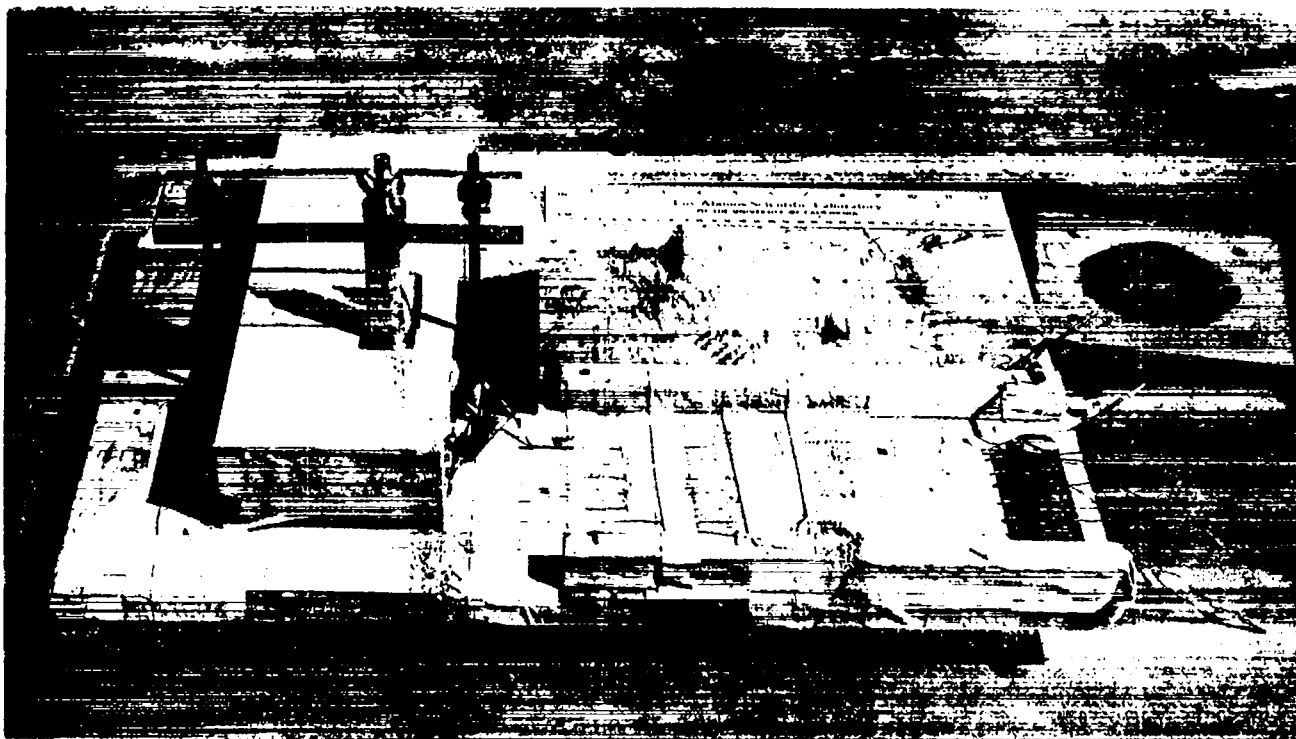Fig. 1. Cross section of a small-scale test.

Fig. 2. Photograph of a small-scale experiment. The witness plate was covered with tape, except in the immediate vicinity of the charge, in order to protect the surface for subsequent experiments.

until it contacted the witness plate, inserting a 0.051-mm-diameter enameled copper wire through holes previously drilled in the tube, adding a drop of light mineral oil (to minimize jetting along the tube wall), inserting the next pellet, inserting another wire, and so on until all of the pellets were loaded. A booster of pressed TNT and an SE-1 detonator were added. The assembly was planned so that when the detonator was seated the column of pellets was compressed to a length equal to the sum of the lengths of the individual pellets. An insulated box and the large heat capacity of the assembly ensured that all charges were fired within 1°C of the assembly room temperature of 23°.

Transit-time signals were obtained by electrical conduction between the small copper wires which extended across the explosive (see Fig. 1) and the brass tube via the reaction products. The signals were recorded on eight raster oscilloscopes operated in parallel and having a time resolution of about 3 ns. A knowledge of the individual pellet lengths and the measured times permitted determination of

the rate by means of a linear least-squares fit to the position-time data.

All charges were fired against two large witness plates, (Fig. 7) which had been prepared from a single piece of 1019 steel. The diamond point hardness was Rockwell B-83 ± 2. Charge spacing was such that any dent was not affected by its neighbors.

Compositions studied in the large-scale experiments were selected on the basis of results obtained in the above described screening experiments. The performance of three compositions was studied in 100-mm-diameter copper cylinder tests. Two cylinder tests were performed for each of the three compositions; one cylinder had a wall thickness of 10.2 mm and the other had a thickness of 5.08 mm. These thicknesses span the charge mass to case mass ratio of most munitions as discussed by Hershkowitz and Akst.[7] Each cylinder was 900 mm long. The copper cylinders were prepared from OFHC brand copper to a tolerance of 0.05 mm on the diameters, and were annealed to a hardness of Rockwell F-50. The cylinders were measured and weighed, then the charge diameter

3

was specified so that: (1) the charge could be assembled in the cylinder, and (2) the ratio of explosive volume to copper mass would be as close to that desired as practicable.

After the charges were prepared, they were assembled in the cylinders by a process similar to that used to assemble the small-scale tests (except that there were no interior switch wires). Witness plates of 1019 steel, 305 mm square by 152 mm thick, and back-up plates were initially used in an attempt to obtain dent data. The rate was measured by means of twelve 0.05-mm-diameter wire switches mounted at known spacing on the exterior of the copper cylinder. Photographs of an assembly and shot are reproduced in Figs. 3 and 4.

The slit of a smear camera was imaged at a location six charge diameters from the booster end of the cylinder. Collimated back-light permitted the smear camera, writing at 0.9 mm/μs, to record the wall motion of the copper cylinder as a function of time. Figure 5 is a reproduction of a smear-camera record.

Position-time data from the exterior wire switches were linear least-squares fitted to obtain the detonation velocity. Position-time data from the smear-camera record were fitted with both a seventh-order polynomial and with a spline-fit routine (see Appendix C) developed specifically for cylinder tests. The cylinder wall velocity as a function of expansion radius was obtained from these fits.
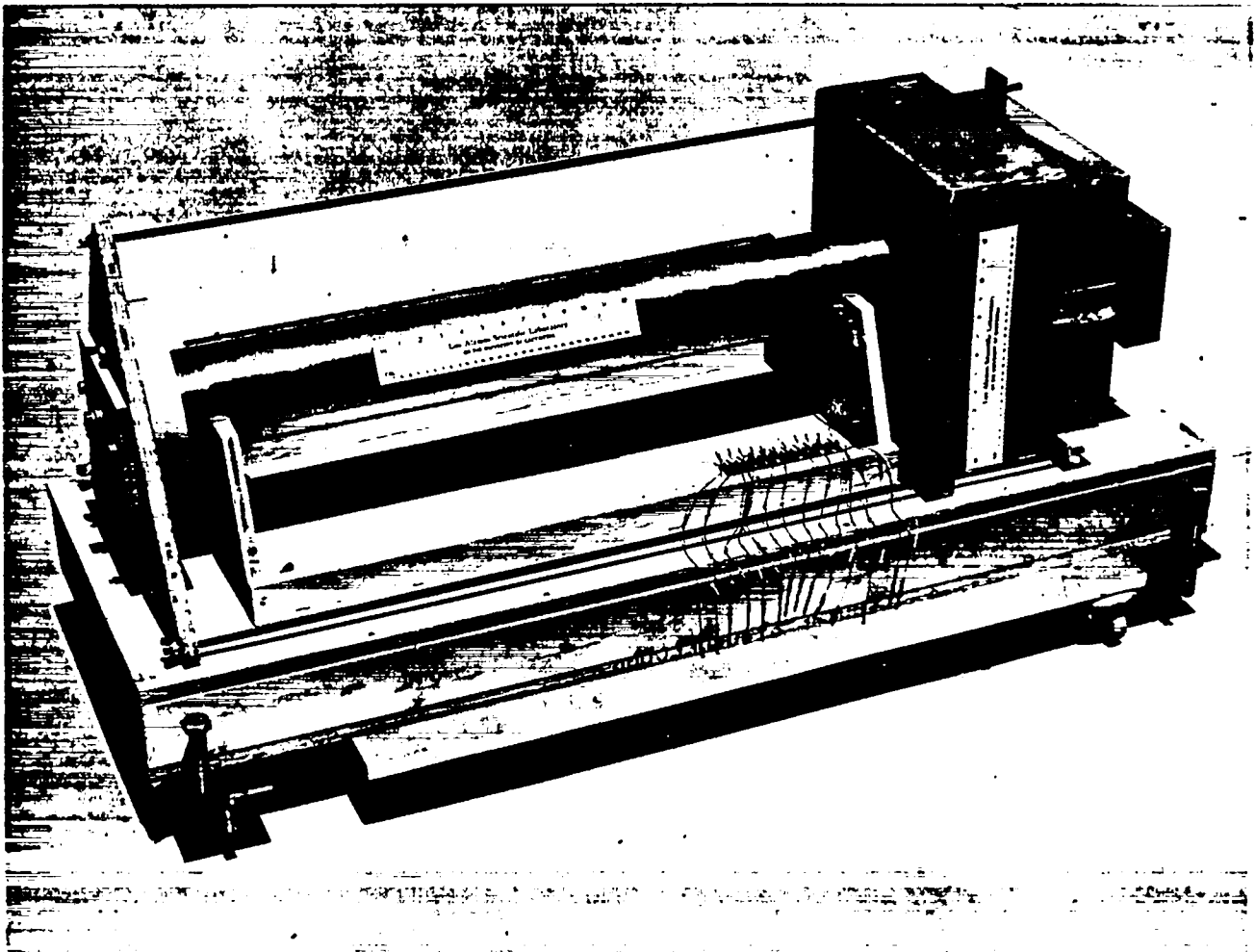

Fig. 3. Close-up of a large-scale cylinder, rate, and plate-dent test.
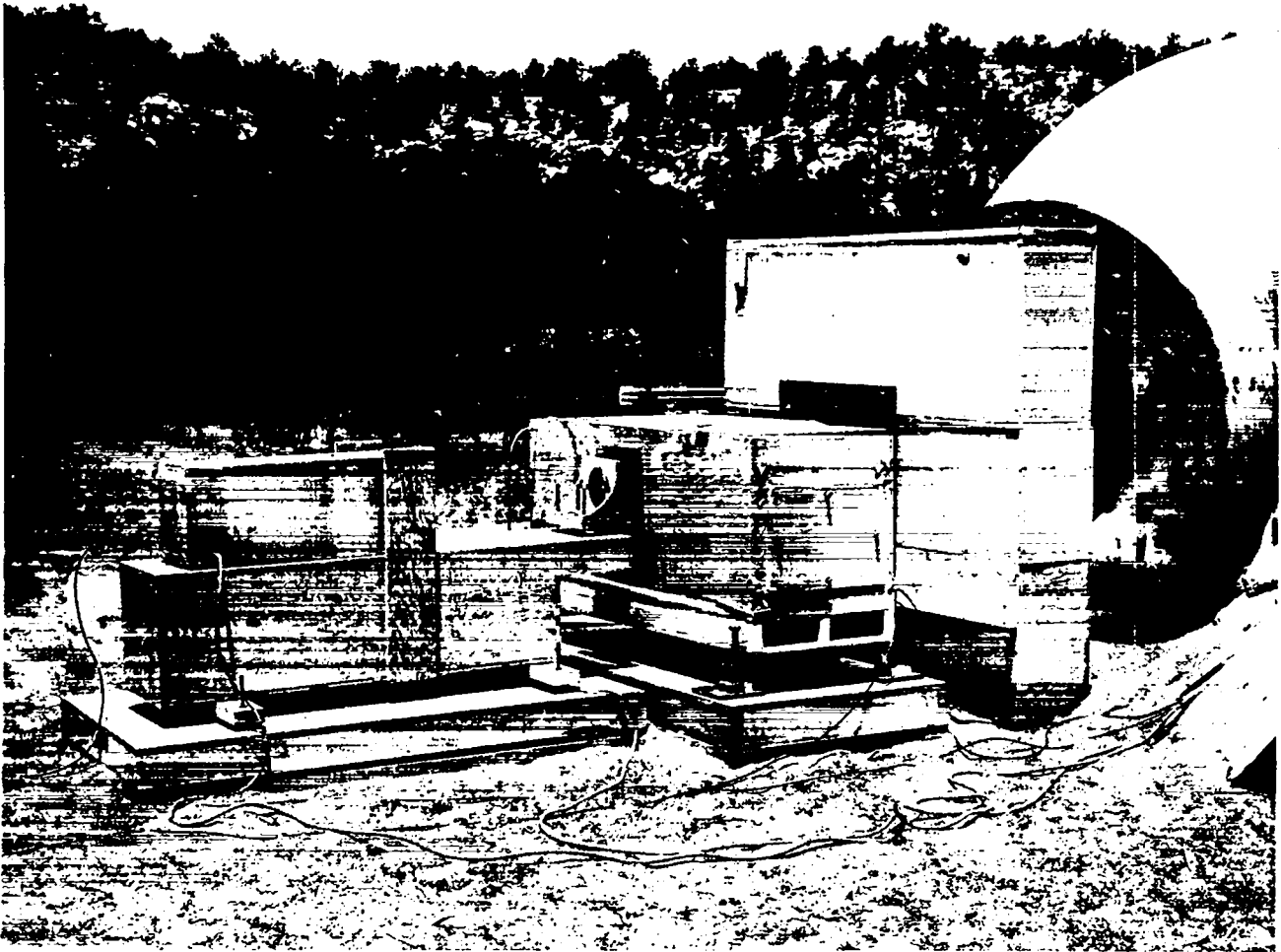
4

Fig. 4. Overall view of a large-scale cylinder, rate, and plate-dent test ready for firing.
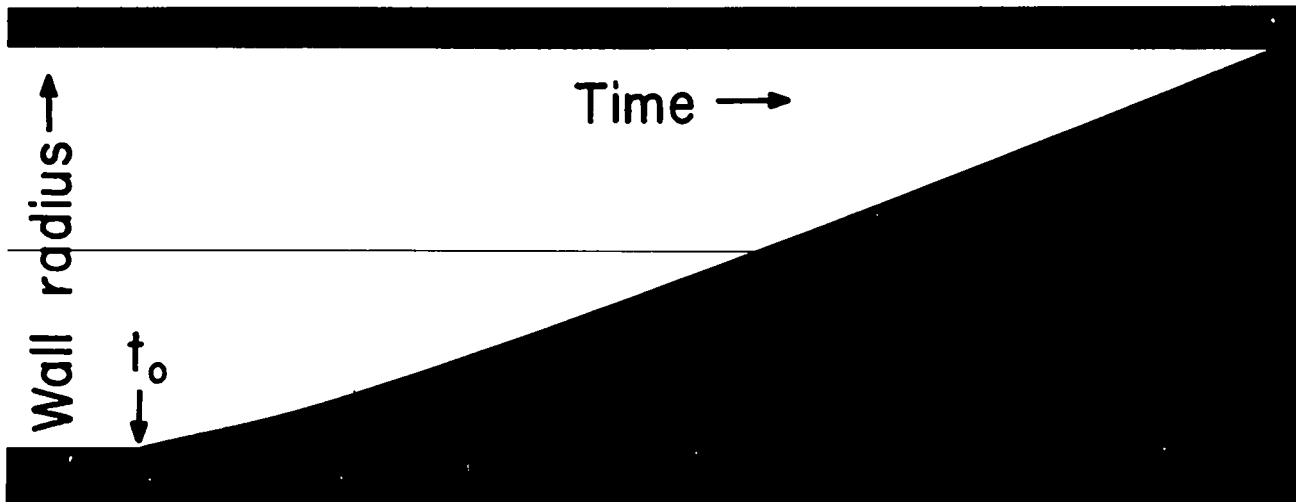
Fig. 5. Smear-camera record obtained in a large-scale cylinder test. Only one side of the cylinder expansion was observed in order to obtain the desired space resolution. Initial motion occurs at time t_o.

III. DATA

A. Experimental

The data obtained in the small-scale tests are summarized in Table I. The charges of 100% RDX, RDX/AN, RDX/MAN, and 100% TNT were fired for the purpose of obtaining reference data. Detonation velocity and dent depth are plotted as a function of the weight percent of either MAN or QMAN in Fig. 6. The two detonation velocity points for RDX/ (MAN + AN) (Shots F-3745 and R-3747 in Table I) that fall well below the curve for that formulation were prepared by first cosolidifying a eutectic of AN and MAN and then blending and grinding with additional AN (see Appendix A for a fuller description of differences in formulations). Figure 7 shows the appearance of the dents obtained in the small-scale tests.

The data of Fig. 6 show that the performance of the MAN formulation increases, as measured by either detonation velocity or by plate dent, essentially until the approximate CO balance is reached (32% in Fig. 6). The performance of the QMAN formulation also increases as measured by plate dent until a CO balance is reached (12% in Fig. 6); however, the detonation velocity decreases as the percent of QMAN increases. The density falls as the percent of either MAN or QMAN increases (assuming a constant percent of voids).

An attempt was made to find a correlation between $\rho_o D^2$ and dent depth as observed for ideal explosives in large-scale dent tests by Smith.[9] The results of our effort to find a correlation are shown in Fig. 8.

The data obtained in the 100-mm-diameter copper cylinder tests are summarized in Table II and in Appendix D. Data for Composition B, Grade A, are included for comparison. The detonation velocities appear to be independent of "thick" or "thin" confinement; i.e., the confinement appears to be effectively infinite. Accordingly, the detonation-velocity data from both small- and large-scale experiments were used to construct Fig. 9. Note that the compositions used for the cylinder tests were prepared (see Appendix A) by blending the eutectic of MAN + AN with additional AN. It appears from the limited data of Fig. 9 that the formulations so prepared have a greater diameter effect than 40 RDX/60 AN. However, the relative effect is reversed when the MAN is cosolidified with all of the AN (assuming the infinite-diameter velocity is independent of the preparation method).

The explosive fills extended 0.5 mm beyond the copper cylinders and were terminated by witness plates in an attempt to obtain large-scale dent data similar to that obtained in the small-scale tests. The witness plate for the first two shots consisted

TABLE I

SUMMARY OF SMALL-SCALE TEST DATA

Composition (wt%)	Shot No.	ρ^a (Mg/m^3)	% Voids	D^a (mm/µs)	Dent^b (mm)	
100 RDX	F-3660	1.737	3.6	8.656	3.58	
100 RDX	C-4466	1.737	3.6	8.587^c	3.61	
40 RDX/60 AN	F-3662	1.703	3.1	7.174	1.89	Large^d AN
40 RDX/60 AN	F-3661	1.701	3.2	7.174	1.93	Large AN
40 RDX/60 AN	F-3743	1.702	3.2	7.118	2.21	Standard^d AN
40 RDX/15 MAN/45 AN	C-4459	1.666	2.1	7.340	2.97	MAN/AN melt
40 RDX/15 MAN/45 AN	C-4458	1.667	2.1	7.311	2.97	MAN/AN melt
40 RDX/15 MAN/45 AN	F-3747	1.660	2.5	7.072	2.96	Eutectic melt
40 RDX/30 MAN/30 AN	F-3664	1.622	1.7	7.491	3.05	MAN/AN melt
40 RDX/30 MAN/30 AN	F-3666	1.622	1.7	7.514	3.07	MAN/AN melt
40 RDX/30 MAN/30 AN	F-3745	1.617	2.0	7.159	2.99	Eutectic melt
40 RDX/45 MAN/15 AN	F-3667	1.571	1.8	7.566	2.97	MAN/AN melt
40 RDX/60 MAN	F-3668	1.527	1.7	7.374	2.84	
40 RDX/60 MAN	F-3671	1.526	1.8	7.272	2.84	
20 RDX/80 MAN	F-3672	1.455	2.0	6.414^c	2.57	Odd-shaped dent
20 RDX/80 MAN	F-3673	1.455	2.0	6.486^c	2.72	
40 RDX/12 QMAN/48 AN	C-4460	1.635	2.7	6.990	2.41	QMAN/AN melt
40 RDX/12 QMAN/48 AN	C-4461	1.635	2.7	7.057	2.36	QMAN/AN melt
40 RDX/20 QMAN/40 AN	C-4462	1.589	2.6	6.937	2.29	Odd-shaped dent
40 RDX/20 QMAN/40 AN	C-4463	1.587	3.0	6.972	2.46	QMAN/AN melt
40 RDX/30 QMAN/30 AN	C-4464	1.531	3.8	6.766^c	2.21	QMAN/AN melt
40 RDX/30 QMAN/30 AN	C-4465	1.532	3.8	6.855	2.21	QMAN/AN melt
100 TNT	F-3741	1.581	4.4	6.920	2.53	
100 TNT	F-3742	1.582	4.4	6.923	2.57	

$^a\rho$ = initial density of charge, D = detonation velocity.

^{b}Dent in steel with a hardness of Rockwell B-83.

^{c}Larger than typical standard deviations and fewer than typical pin signals.

^{d}Large AN was prepared by crushing prills with mortar and pestle; the particle size was not characterized. Standard AN had a median particle size of 40µm and the distribution is described in Table A-3, Appendix A.

of a 150-mm-thick by 360-mm-square boiler plate plus a 50-mm-thick spall plate. The witness plate fractured on the second shot; thereafter, a 100-mm-thick back-up plate was inserted between the witness and spall plates. Even with the back-up plate, some of the witness plates fractured. Furthermore, there is evidence of massive interior failure even when the witness plate did not fracture. The dent tests with thick- and thin-walled cylinders yielded inconsistent data. In view of these complications, the plate-dent data obtained with the cylinder shots must be considered invalid. The value of the plate-dent test remains unchanged for the small-scale tests or for the unconfined explosive dent test of Smith[9], since in both of these cases the stress-time function applied to the plate is far less severe.
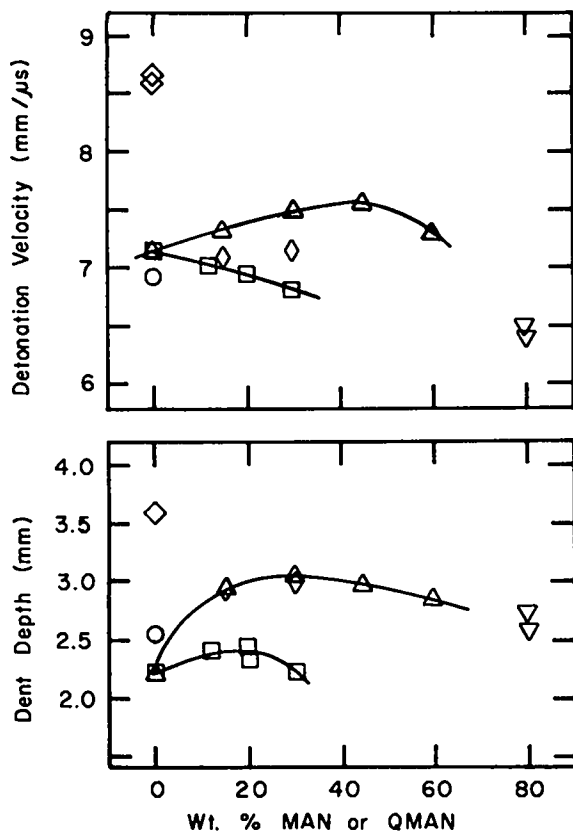
◇ 100 RDX   △ 40 RDX / 60 (MAN +
▽ 20 RDX / 80 MAN   AN Melt)
O 100 TNT (pressed)   □ 40 RDX / 60 (QMAN +
     AN Melt)

◊ 40 RDX / 60 (MAN + AN Eutectic Melt + AN)

Fig. 6. Detonation velocity and dent depth from
small scale experiments as functions of
wt% MAN or QMAN with RDX constant at 40
wt% and with AN completing the formulation
except as noted. Data obtained with
charges containing "large" AN are not
plotted. The CO balance for MAN + AN alone
occurs when the wt ratio of MAN/AN is 54/
46; the ratio for QMAN / AN is 20/80.

The cylinder wall velocities were analyzed in
two ways: by fitting the position-time data with a
seventh-order polynomial, and by a cubic spline me-
thod. A brief discussion of the spline technique is
given in Appendix C.

The thin wall cylinder filled with 40 RDX/15
MAN/45 AN ruptured early, so data at the 76-mm
expansion were not obtained. Accordingly, an effort
was made to determine if the ratio of wall energy
between thick- and thin-wall cylinders with the same
fill could be considered a constant. The results of
this ratio test at expansions of 20 and 76 mm are
given in Table II. Ratios for various expansions are
plotted in Fig. 10. All of the ratios fall within
1% of the mean.

The ratios of wall kinetic energies, determined
from the seventh-order polynomial fits, for the two
MAN formulations relative to that for 40 RDX/60 AN
are plotted in Figs. 11 and 12. A plot of the wall
kinetic energies for both MAN formulations, for 40
RDX/60 AN, and for Amatex 40 (40 RDX/40 TNT/20 AN),
all normalized to 65 RDX/34 TNT/1 WAX wall energy, is
given in Fig. 13.

B. Calculations

The results of idealized (assuming total reac-
tion) calculations using the TIGER program[11] are
summarized in Table III. If 40 RDX/60 AN and cer-
tain other formulations reacted ideally they would
have CJ pressures and detonation velocities in ex-
cess of those of Composition B. Pertinent detona-
tion velocities and pressures are plotted in Fig.
14; the format and scales are similar to those used
to display the data obtained in small-scale experi-
ments. The data calculated for formulations of MAN
and QMAN (ideal values) extrapolate in a monotoni-
cally increasing manner to that for 40 RDX/60 AN in
contrast to the experimental data obtained in the
small-scale experiments (Fig. 6), where generally
peaks occur with substitution of MAN or QMAN.

Calculations were also performed with the BKW
program using a technique for varying the fraction
of AN reacted.[6] Any fraction of AN may be treated
as inert, but the balance reacts to equilibrium at
the CJ plane. These calculations were restricted
to formulations and densities tested in the large-
scale experiments. Results of the BKW calculations
are summarized in Table IV. Selected results are
plotted in Fig. 15.
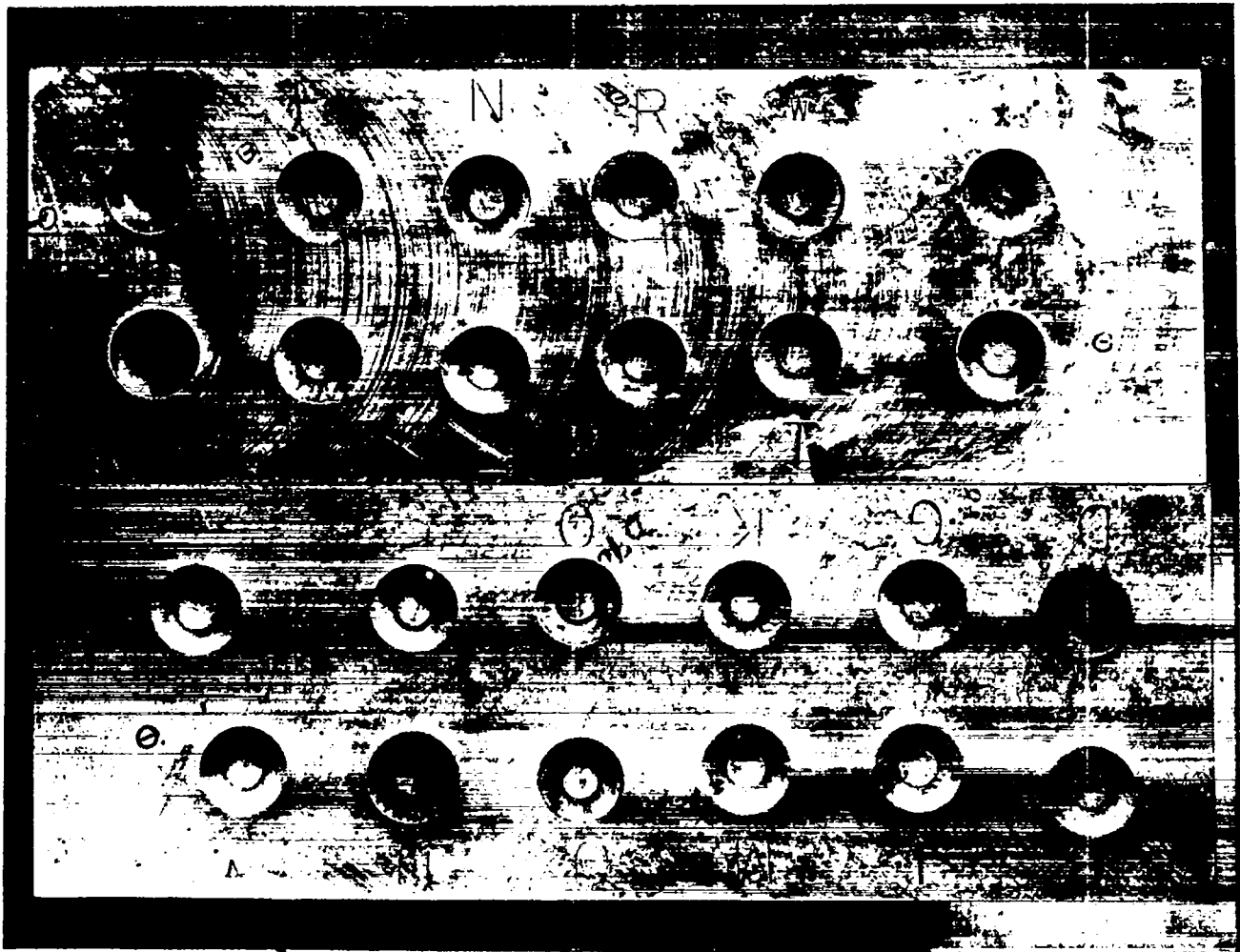
Fig. 7. Photograph of the dents produced in the small-scale tests.

Fig. 9. Approximate diameter effect assuming the confinement in both small- and large-scale tests is essentially infinitely thick.

Fig. 8. Correlation between $\rho_0 D^2$ and dent depth for small-scale tests. Only the data for RDX/MAN/AN are sufficient to establish a correlation and that correlation is clearly limited to that formulation. The family of dashed lines is intended to suggest a possible family of correlations.
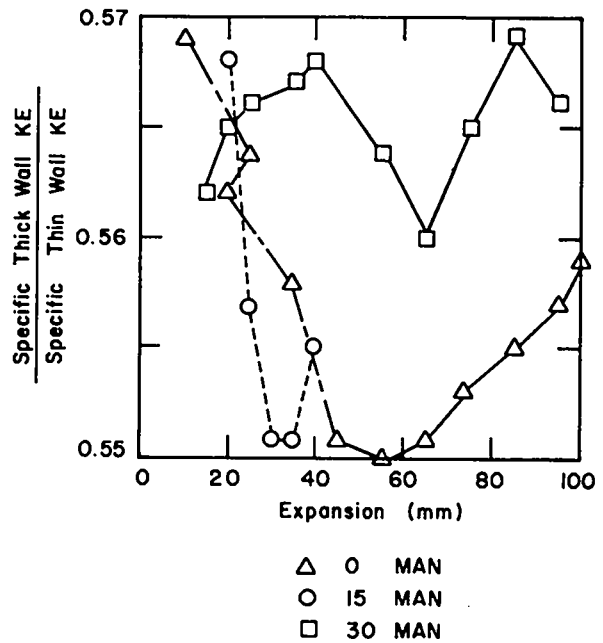
Fig. 10. Ratio of the square of the wall velocities for thick- and thin-wall cylinders as a function of cylinder expansion. Note the expanded scale and the generally random distribution from the mean. The mass of the cylinders would have to be taken into account to determine the relative energy imparted by the same volume of explosive.

TABLE II

SUMMARY OF DATA OBTAINED FROM CYLINDER TESTS

Shot No.	RDX	MAN	AN	ρ₀ (Mg/m³) [b]	% Voids	Thickness (mm)	Velocity at 20 mm (mm/μs)	Ratio V20 [d]	Relative Energy E20 [e]	Velocity at 76 mm (mm/μs)	Ratio V76 [d]	Relative Energy E76 [e]	D (mm/μs) [f]	σ (mm/μs) [g]
		Composition[a]								Cylinder[c]				
C-4508	40	–	60	1.720	2.2	10.2	1.325	–	0.93	1.534	–	0.89	7.584	0.004
								0.752			0.744			
C-4506	40	–	60	1.720	2.2	5.1	1.761	–	h	2.063	–	h	7.592	0.004
C-4510	40	15	45	1.673	1.7	10.2	1.348	–	0.95	1.572	–	0.93	7.637	0.003
								0.752						
C-4509	40	15	45	1.672	1.8	5.1	1.793	–	h	Lost[i]	–	Lost[i]	7.651	0.002
C-4511	40	30	30	1.631	1.1	10.2	1.360	–	0.98	1.589	–	0.95	7.880	0.002
								0.752			0.752			
C-4512	40	30	30	1.630	1.2	5.1	1.809	–	h	2.112	–	h	7.883	0.003
C-4430	65 RDX/34 TNT/1 Wax			1.696	2.5	10.2	1.333		1.0	1.597		1.0	7.867	0.007
LLL[k]	Composition B, Grade A[j,k]			1.717	1.3	10.4	1.39	1.04	1.07	1.63	1.02	1.04		
C-4374	64 RDX/35 TNT/1 Wax[j]			1.701	2.2	10.3	1.38	1.04	1.07	1.63	1.02	1.04	7.915	0.002

[a] Nominal composition in wt%.

[b] Initial density.

[c] 101.6-mm diameter; not scaled.

[d] Ratio of velocities of thick and thin-wall cylinders at expansion indicated, velocities determined by either a seventh-order polynomial or a fit to low-order spline (7 or 8 knots).

[e] Cylinder-wall energy relative to that of Composition B (Shot C-4374) at the expansion indicated (scaling assumed).

[f] Detonation velocity.

[g] Standard deviation for D.

[h] No thin-wall data are available for Composition B.

[i] Cylinder ruptured early.

[j] Scaled to 100-mm diameter from 25-mm-diameter experiment.

[k] Average of scaled 25-mm- and 50-mm-diameter experiments reported in Ref. 11.
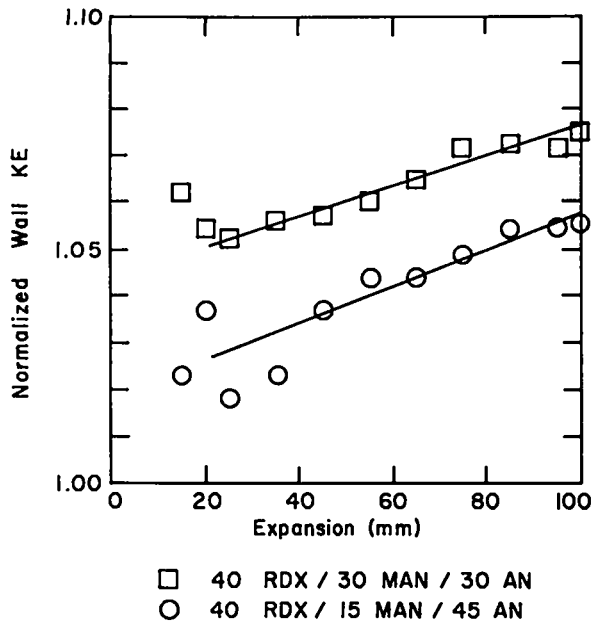
Fig. 11. Cylinder wall kinetic energies for MAN
formulations normalized to 40 RDX/60 AN
(all 10.2-mm-thick walls).
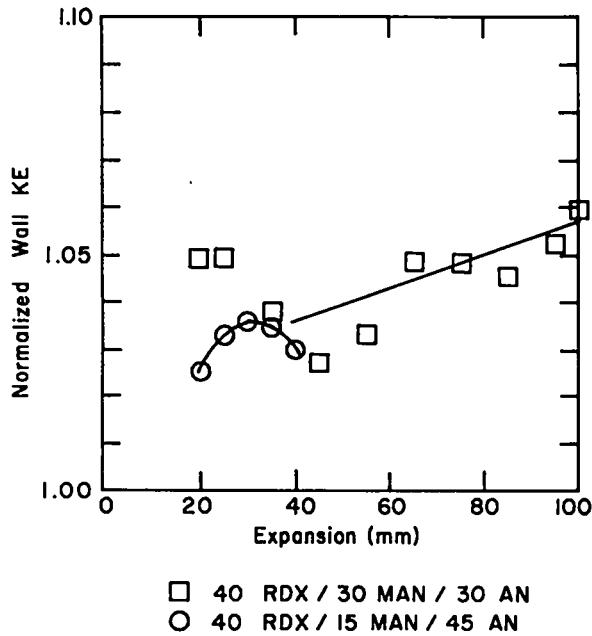
Fig. 12. Cylinder wall kinetic energies for MAN
formulations normalized to 40 RDX/60 AN
(all 5.1-mm-thick walls).

△ 40 RDX / 60 AN
◇ 40 RDX / 40 TNT / 20 AN
○ 40 RDX / 15 MAN / 45 AN
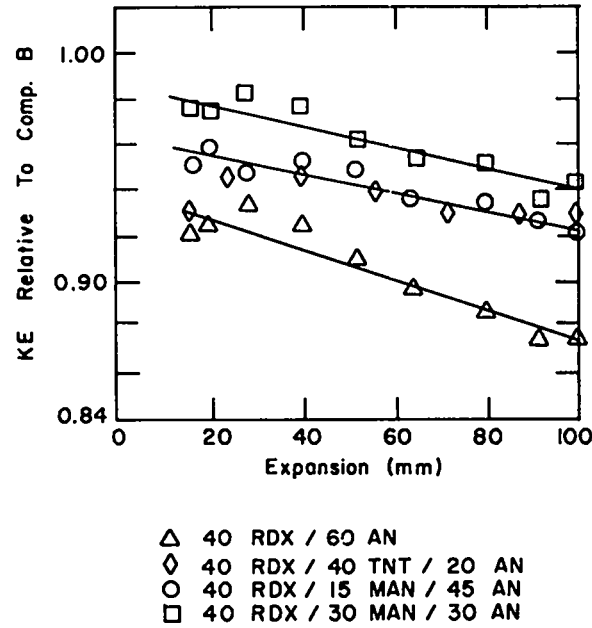□ 40 RDX / 30 MAN / 30 AN

Fig. 13. Cylinder wall kinetic energies normalized
to Composition B, Grade A, shot C-4374
which gave data essentially identical to
that reported by LLL[10] (all 10.2-mm-thick
walls).

TABLE III

TIGER PREDICTIONS OF EXPLOSIVE PROPERTIES

Composition by weight %				Density	D	P	T	$\rho\Delta E^d_{2V_o}$		$\rho\Delta E^d_{7V_o}$	
RDX	MAN	QMAN	AN	Mg/m^3	$(mm/\mu s)$	(GPa)	(K)	$\frac{Mg}{m^3}$	$\frac{Cal}{g}$	$\frac{Mg}{m^3}$	$\frac{Cal}{g}$
100	--	--	--	1.802	8.774	34.2	2631	--		--	
100	--	--	--	1.740[a]	8.534	31.5	2759	--		--	
--	--	--	100	1.725[b]	7.84	20.7	470[c]	--		--	
--	100	--	--	1.420[b]	7.51	19.3	1733	979		1341	
--	--	100	--	1.250[b]	7.21	15.5	1403	--		--	
40	--	--	60	1.700[a]	8.560	28.9	1565	--		--	
40	--	--	60	1.720[a]	8.651	29.7	1529	1444		1861	
40	60	--	--	1.525[a]	7.888	23.3	2121	--		--	
20	80	--	--	1.454	7.632	20.7	1946	--		--	
40	15	--	45	1.702	8.680	30.2	1741	--		--	
40	15	--	45	1.673[a]	8.550	28.9	1795	1449		1923	
40	15	--	45	1.665[a]	8.515	28.6	1810	--		--	
40	30	--	30	1.625[a]	8.329	27.0	1908	--		--	
40	30	--	30	1.631[a]	8.355	27.3	1898	1376		1852	
40	30	--	30	1.650	8.437	28.0	1863	--		--	
40	45	--	15	1.570[a]	8.085	25.0	2027	--		--	
40	--	12	48	1.635[a]	8.353	27.3	1856	--		--	
40	--	20	40	1.590[a]	8.133	25.5	1943	--		--	
40	--	30	30	1.535[a]	7.865	23.2	2039	--		--	
100 TNT				1.630	6.930	19.9	2921	1062		1541	
64 RDX/36 TNT				1.717	8.103	28.1	2781	1454		2043	
60 RDX/40 TNT				1.686	7.952	26.7	2829	--		--	

a) Experimental densities for either small scale tests or cylinder tests.
b) Theoretical densities.
c) The low T suggests the possibility of a difficulty with the BKW equation of state.
d) $\rho\Delta E$ is the product of the density and the difference in energy per unit weight at the expansion indicated by the subscript and the heat of formation at standard conditions.
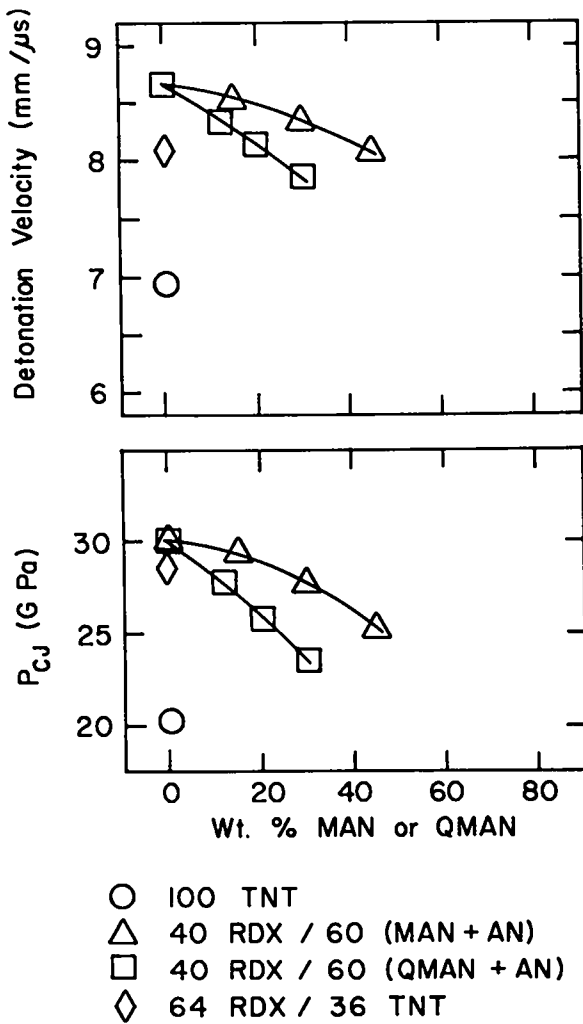
Fig. 14. TIGER calculations of CJ pressure and detonation velocity as a function of wt % MAN or QMAN with RDX constant at 40% and AN completing the formulation except as noted.

Legend for Fig. 14:
○ 100 TNT
△ 40 RDX / 60 (MAN + AN)
□ 40 RDX / 60 (QMAN + AN)
◇ 64 RDX / 36 TNT

Legend for Fig. 15:
△ 40 RDX / 60 AN
○ 40 RDX / 15 MAN / 45 AN
□ 40 RDX / 30 MAN / 30 AN
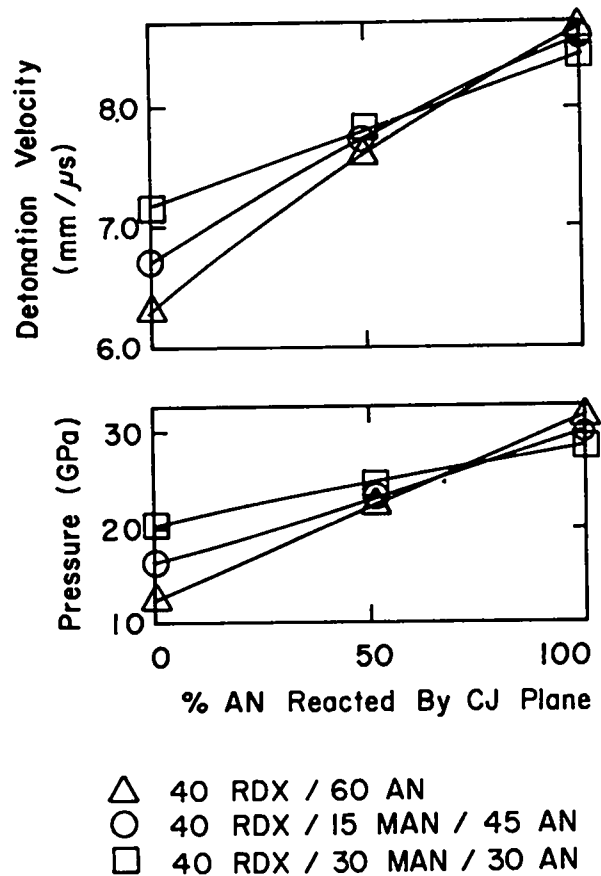
Fig. 15. BKW calculations of CJ pressure and detonation velocity as a function of wt % AN reacted.

TABLE IV

BKW PREDICTIONS OF CJ PROPERTIES

Composition by wt %			Density	Fraction AN Reacted	D_{CJ}	P_{CJ}	T_{CJ}	Gamma $\frac{d\ell nP}{d\ell nV}$	$D_{experimental}$[a]	ΔD[c]
RDX	MAN	AN	(Mg/m^3)		$(mm/\mu s)$	(GPa)	(K)		$(mm/\mu s)$	$(mm/\mu s)$
40	--	60	1.720	0	6.153	13.8	1244	3.722		
				0.5	7.592	22.6	1547	3.376	7.588	-0.004
				1.0	8.676	30.8	1591	3.192		
40	15	45	1.673	0	6.698	16.8	1470	3.472		
				0.481[b]	7.644[b]	22.9[b]	----	-----	7.644	0
				0.5	7.691	23.2	1689	3.262	7.644	-0.047
				1.0	8.566	29.9	1837	3.099		
40	30	30	1.631	0	7.186	19.7	1690	3.282		
				0.5	7.801	23.8	1827	3.162	7.882	0.081
				0.57[b]	7.882	24.4[b]	----	----	7.882	0
				1.0	8.367	28.1	1931	3.054		

---

a   100-mm diameter, confined by copper.

b   Obtained by interpolation using Fig. 15.

c $D_{experimental}$ minus D_{CJ}.

IV. DISCUSSION

The detonation velocity of 40 RDX/60 AN, the reference explosive for this study, in small and large confined charges is well below its potential. The experimental performance is such that the energy imparted to a cylinder wall is about 0.9 that imparted by Composition B (Fig. 13) while the ratio of ideal detonation pressures is 1.1 (Table III). The experimental infinite-medium detonation velocity is near 7.6 mm/μs (Fig. 9) while the calculated velocity, based on an assumption of total reaction, is between 8.6 and 8.8 mm/μs (Tables III and IV).

The effects of partial substitution of the nondetonable fuel, QMAN, for AN in the reference explosive are shown in Fig. 6. Cosolidification of QMAN with AN improved the performance as measured by the small-scale dent test. The plate-dent depth peaked near the CO balance; density decreased as the QMAN increased. The detonation velocity also decreased as the percent QMAN increased. The QMAN is nondetonable. The detonation velocity decreased with increasing QMAN, and addition of a nondetonable is expected to increase the diameter effect if the particle size remains unchanged. The RDX particle size was controlled. It is reasonable to attribute the increased plate dent to a synergistic effect between AN and QMAN. Additional support for a synergistic effect is provided by calculations that assume total reaction but do not predict the observed peak in performance (Figs. 6 and 14). However, the velocity defect [the difference between the calculated (ideal) and observed detonation velocities] is large as shown in Fig. 16.

The substitution of the detonable fuel, MAN, for AN in the reference explosive also improved performance. Both plate dent and detonation velocity were improved in small scale (Fig. 6). Detonation velocity appears to be a function of the proportion cosolidified, i.e., a function of the way the formulations were prepared (eutectic melt plus AN vs noneutective melt). There also may have been a difference in the cooling rates. The dent test did not distinguish between the two methods of preparation. The plate dent peaked near the CO balance. Detonation velocity and dent data are not sufficient to conclude that a
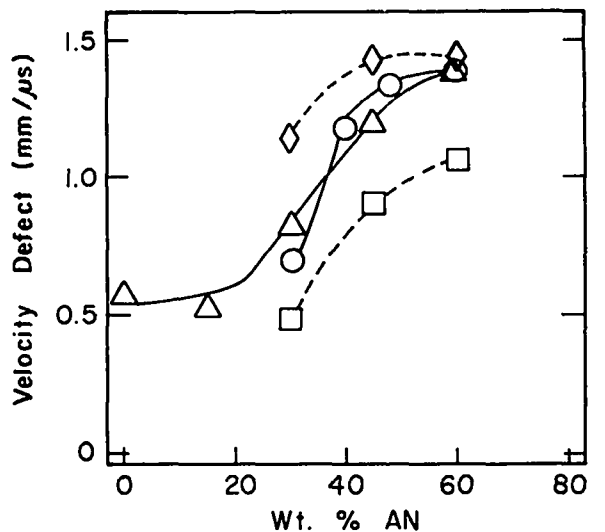
◇ 40 RDX / 60 (Eutectic MAN / AN + AN) small scale

△ 40 RDX / 60 (MAN / AN) small scale

○ 40 RDX / 60 (QMAN / AN) small scale

▢ 40 RDX / 60 (Eutectic MAN / AN + AN) large scale

Fig. 16. The effect of replacing AN with MAN or QMAN on the velocity defect, i.e., the difference between calculated and experimental detonation velocities.

synergistic effect was observed, because the detonability of MAN may have resulted in a diameter effect that produced the observations.

It has been shown that dent depth from medium-scale tests (38-mm diameter by 6 diameters long) correlates with measurements of detonation pressure in large-scale tests.[9] The ratios of the dent depths reported herein to those reported by Smith are 0.38 and 0.34 to TNT and RDX, respectively. This suggests linear scaling; however, additional tests with other explosives are needed to establish a scaling factor. If the dent depth were linearly related to detonation pressure, all of the data plotted in Fig. 8 should define a single straight line. This is not the case.

The data plotted in Fig. 9 show that all of the MAN formulations studied show a significant diameter effect. The diameter effect apparently increases as the percent MAN increases. The

formulations prepared from the eutectic show a larger diameter effect than the reference formulation (40 RDX/60 AN). The method of preparation does not usually affect the detonation velocity of large charges as much as small charges. If this is the case for the MAN formulations, the formulations prepared by the noneutectic method have a diameter effect similar to that of the reference formulation. Accordingly, the diameter effect appears to be either unchanged or in the opposite direction to account for the improvement in small-scale performance as MAN is substituted for AN.

The kinetic energy imparted to a copper cylinder increased as the percent of MAN substituted for AN increased (Figs. 11 through 13). To a first approximation this effect is independent of the wall thickness; the ratio of the kinetic energies for 10-mm:5-mm-thick copper walls is 0.56 ± 0.01 for all expansions (Fig. 10). The positive slopes of the normalized wall energies shown in Figs. 11 and 12 suggest that the addition of MAN does increase the reaction of AN as time increases relative to RDX/AN. The magnitude of the effect is well beyond experimental error.

Mader has demonstrated that a correlation exists between the CJ pressure as calculated by BKW and the experimental cylinder wall velocity for a variety of ideal explosives.[6] He has also found an empirical method, viz., treating an appropriate portion of AN as an inert, which leads to correlation within 4 GPa for nonideal explosives that contain AN. Figure 17 shows the correlation for ideal explosives and data obtained in this study.

The data of Fig. 15 can be used to show that the displacement for RDX/MAN/AN from the ideal explosive correlation curves cannot be attributed to diameter effect as proposed in reference 6, even when the associated increase in cylinder velocity is ignored.

The velocity-defect data for the large- and small-scale tests are plotted in Fig. 16. The large velocity defect for the formulation richest in AN exemplifies the problem with composite explosives. The experimental performance is far below the potential. The velocity defect decreases significantly as AN is replaced with MAN. Nonetheless, the velocity defect is significant for either TIGER or BKW calculation, which assume ideal reaction.
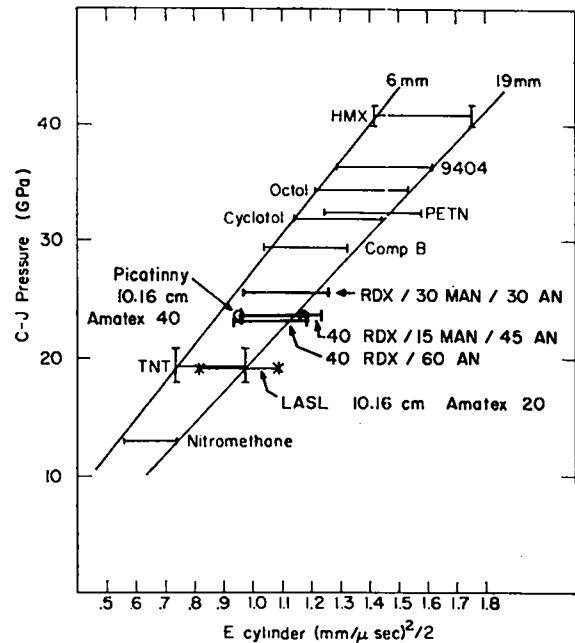
Fig. 17. Correlation between BKW-calculated CJ pressure and cylinder wall energy at two expansions (all scaled to the standard 25-mm-diam cylinder).

The BKW calculations, in which about 50%, 48%, and 57% of the AN were assumed to react in order to reproduce the experimental detonation velocities, respectively, for 40 RDX/60 AN, 40 RDX/15 MAN/45 AN, and 40 RDX/30 MAN/30 AN, suggest that the equivalent of those percents of the AN reacted quickly enough to affect the detonation velocity. It does not mean that only 50% of the AN ultimately reacted. An attempt to recover AN from the products of explosives containing AN proved that the AN ultimately decomposed when subjected to the conditions of a closed bomb.[12] Furthermore, it is not known that MAN reacts ideally as is assumed in the BKW calculations.

The model proposed by Mader can be used to argue that the substitution of 15% MAN for AN may have slightly decreased the fraction of AN reacted ahead of the CJ plane relative to 40 RDX/60 AN; but the small decrease is within the uncertainties. Conversely, substitution of 30% MAN for AN apparently increased the fraction of AN reacted ahead of the CJ plane. However, since the percent of AN decreased more than the

fraction of AN that reacts quickly increased, the model implies that the mass of AN per unit volume that reacts decreased as AN is replaced with MAN. This observation is contrary to intuition which suggests that a greater fraction of the oxidizer would react as the oxygen decreased, fuel increased, and temperature increased (Table IV).

It has been established that the detonation velocity of an ideal composite explosive can generally be expressed as a volume fraction weighted sum of the Urizar constants of the components, where these constants are the detonation velocities for ideal explosive components and are experimentally determined for inerts or estimated from the density of the inert.[13,14] The defining equation can be inverted, when the experimental detonation velocity of a composite and of all explosive components but one are known, to determine the Urizar constant of the remaining component. This was done for AN in the compositions in which MAN was substituted for AN to see if an increasing trend for the Urizar constant of AN was present as the MAN component was increased. In this calculation it was assumed, without evidence, that the MAN explosive did not change and that it could be represented by the TIGER-calculated value of $D = 7.512$ mm/μs. The results of the calculation are shown in Table V. It was concluded that the calculation showed that there was an increase in the effective detonation velocity only for the formulation with 30% MAN. This does not depend on the particular value of D used for MAN, but it does depend on the same value acting throughout. This model cannot identify reaction behind the CJ plane.

It was next proposed to try to extend the Urizar coefficient concept to kinetic energy imparted to the wall at a sevenfold explosive volume expansion in the standard cylinder test.[14] Thus, it would be asserted that the wall kinetic energy for a composite ideal explosive is a volume weighted sum of that obtained in cylinder tests of the pure components. This assertion remains to be proved by separate experiments and calculations with a series of other explosives. Assuming the hypothesis is correct, then in analagous fashion to the procedure used to obtain an "effective detonation velocity" for AN in the MAN-for-AN series, one can

calculate an "effective kinetic energy" (EKE) for AN. The result of these calculations is shown in Table VI. The EKE for AN shows a progressive increase as MAN is substituted for AN. The trend does not depend on the precise value used for MAN but it does depend on it being constant. It is recognized that the calculations made for "effective detonation velocity" and EKE are only exploratory. However, the results, perhaps fortuitous, do agree with the other data in showing limited synergism in the time scale which affects the detonation velocity and a definite effect for the longer time scale of the cylinder test.

The correlation and data in Fig. 15 can be used to determine a correlation pressure, i.e., the CJ pressure required by the correlation to produce the observed cylinder wall energy. The pressure thus obtained can be compared with the BKW calculation in which all of the AN was reacted. The comparison is made in Table VII. The correlation pressure is essentially independent of the cylinder expansion for which the correlation is made except for the case of 30% MAN at 19-mm expansion. Composite explosives do not appear to perform as much below their potential when compared by the above method as when only the observed and calculated detonation velocities are compared. The difference between the BKW and correlation pressures decreases linearly as a function of either weight or volume percent MAN within the estimated errors. From a plot of the CJ pressure as a function of fraction AN reacted (Table IV) and the correlation pressures (Table VII), the fraction AN reacted can be determined for the time scale that governs the cylinder wall energy at either 6- or 19-mm expansion. The data thus obtained are given in Table VIII. The AN reacted increases linearly from about 61% for 40 RDX/60 AN to as much as 81% for 40 RDX/30 MAN/30 AN at 19 mm of expansion.

V. CONCLUSION

The substitution of detonable MAN for AN in RDX/AN results in a higher detonation velocity and improved plate-dent performance in small-scale tests. Best performance appears to occur when the MAN/AN is balanced to CO and the MAN/AN were cosolidified from the melt. The substitution of non-detonable QMAN for AN in RDX/AN results in a lower detonation velocity but improved plate-dent

TABLE V

CALCULATIONS OF "EFFECTIVE DETONATION VELOCITY"

Weight Percent			Volume Fraction			Experimental[a]		U_{AN}[b]
						ρ_{TMD} (Mg/m^3)	D_{TMD} $(mm/\mu s)$	
RDX	MAN	AN	RDX	MAN	AN			$(mm/\mu s)$
40		60	.3896		.6104	1.7550	7.704	7.022
40	15	45	.3772	.1795	.4433	1.6993	7.731	6.934
40	30	30	.3656	.3480	.2864	1.6470	7.935	7.380

a These values of detonation velocity were obtained from the experimental values by adding 0.33 mm/μs for each 0.1 Mg/m^3 increase in density.

b Urizar constant for AN. Other values used were RDX: ρ = 1.802 Mg/m^3, U = 8.774 mm/μs; MAN: ρ = 1.42 Mg/m^3, U = 7.512 mm/μs.

TABLE VI

CALCULATIONS OF "EFFECTIVE KINETIC ENERGY"

Composition by Wt %			ρ (Mg/m^3)	ρE_{7V_o}[a] $(g/m\mu s^2)$	$\rho \Delta E_{7V_o}$[b] $(Mg/m^3 \ cal/g)$	E_{AN}[c] $(mm^2/\mu s^2)$
RDX	MAN	AN				
40		60	1.720	4.352	1861	1.836
40	15	45	1.673	4.134	1922	2.160
40	30	30	1.631	4.118	1851	2.612

a ρE_{7V_o} is the square of the experimental wall velocities at a seven-fold volume expansion multiplied by density of the condensed explosive.

b $\rho \Delta E_{7V_o}$ is the TIGER calculated change in energy content of the explosive per unit mass between the condensed state and the seven-fold volume expansion point on the isentrope from the CJ state also multiplied by the density of the condensed state.

c E_{AN} is the calculated value in which the RDX effective kinetic energy value used was 3.229 $mm^2/\mu s^2$, derived from cylinder test data on 64 RDX/36 TNT, 77 RDX/23 TNT and TNT (all weight percents). The value for MAN was 1.687 $mm^2/\mu s^2$ derived from TIGER calculations scaled by the proportionality to experimental values and ρ_{AN} = 1.683 Mg/m^3.

TABLE VII

COMPARISON OF BKW AND CORRELATION PRESSURES

Composition by Wt %				Pressure			Pressure		
RDX	MAN	AN	TNT	BKW (GPa)	$2V_\phi$ [a] (GPa)	Δ [b] (GPa)	BKW (GPa)	$7V_o$ [c] (GPa)	Δ [b] (GPa)
40	---	60	---	30.8	24.5	5.3	30.8	23.8	7.0
40	15	45	---	29.9	24.9	5.0	29.9	25.0	4.9
40	30	30	---	28.1	25.2	2.9	28.1	26.5	1.6
40	---	30	30[d]	26.5[e]	25.1	1.4	26.5	23.6	2.9
20	---	40	40[f]	25.0[e]	21.4	3.6	25.0	21.6	3.4

a   Correlation pressure obtained graphically from Fig. 15 by use of the 6-mm correlation line and the cylinder wall energy at 6-mm expansion.

b   BKW (all AN reacted) minus n V_o where n is as indicated.

c   Correlation pressure obtained graphically from Fig. 15 by use of the 19-mm correlation line and the cylinder wall energy at 19-mm expansion.

d   Amatex/40.

e   Reference 6.

f   Amatex/20.

performance in small-scale tests. The density is reduced as either MAN or QMAN is substituted. Accordingly, QMAN and/or MAN has a synergistic effect.

Large-scale tests in which only part of the AN was cosolidified with MAN resulted in the highest detonation velocity and cylinder wall velocity occurring at the CO balance. The observed detonation velocities and the BKW calculations suggest that only about 50% of the AN reacts on a short enough time scale to affect the detonation velocity when no MAN is present (i.e., 40 RDX/60 AN), and about 57% of the AN reacts when the composition contains 30% MAN by weight. There is less AN present in the second case but it reacts more efficiently at early time.

The cylinder wall energy for thick-wall cylinders is 56 $\pm$ 1% of that for thin-wall cylinders at all observed expansions.

Two methods for interpreting the data for cylinder wall energy were presented. The EKE (effective kinetic energy) method leads to the conclusion that the efficiency or completeness of the AN reaction increases significantly at late times in the presence of 30 wt % MAN. The method's parent, the effective detonation velocity method, predicted a detonation velocity vs % MAN curve which is displaced from but parallels the experimental data. The EKE method has not been tested; consequently, conclusions based on this method must be considered suspect until justified.

The second method, the correlation method, leads to the conclusion that the efficiency of the AN reaction for all formulations studied (including 40 RDX/60 AN, Amatex/20, and Amatex/40) increases between the time frame that governs detonation velocity and that which governs cylinder wall velocity at 6-mm expansion. The increase is that expected for reaction of about 10% of the original AN for 40 RDX/60 (AN+MAN) and 20% for the Amatex formulations. An additional increase in the efficiency was observed for 40 RDX/30 MAN/30 AN

TABLE VIII

FRACTION AN REACTED FOR CORRELATION PRESSURE

| Composition by Wt % | | | | $2V_0$ [a] | | $7V_0$ [b] | |
RDX	MAN	AN	TNT	Pressure (GPa)	Fraction AN Reacted	Pressure (GPa)	Fraction AN Reacted
40	---	60	---	24.5	0.61	23.8	0.57
40	15	45	---	24.9	0.63	25.0	0.64
40	30	30	---	25.2	0.65	26.5	0.81
40	---	30	30	25.1	0.77[c]	23.6	0.52[c,d]
20	---	40	40	21.4	0.70[c]	21.6	0.72[c]

a   6-mm expansion correlation

b   19-mm expansion correlation

c   Pressure vs fraction AN reacted obtained from Reference 6.

d   This value appears erroneous, but no error has been found.

at late times; at 19-mm cylinder expansion the increase was that expected for reaction of another 16% of the original AN. Experimental error may have masked a second increase in efficiency for the formulation with 15% MAN and led to a larger than proper second increase for the formulation with 30% MAN. A second increase in efficiency was not observed for 40 RDX/60 AN or for Amatex. The above estimates of the increases in efficiency are suspect in that there may be errors in the equation of state for unreacted AN and for MAN, MAN probably does not react ideally as assumed, and the transfer of energy to the cylinder wall is probably not the same as it is for an ideal detonation as assumed. Nonetheless, these limitations do not invalidate the trends.

It is a fact that 40 RDX/15 MAN/45 AN performs as well as Amatex/40 and that 40 RDX/30 MAN/30 AN outperforms Amatex/40 as measured with the cylinder test. The liquidus temperature for equal weights of MAN/AN is 86°C. On the basis of performance, casting temperature, and cost, it appears that MAN/AN could be substituted for TNT/AN in Amatex.

VI. RECOMMENDATIONS

The idea of improving performance by cosolidification has merit. Fuels other than those used in this study, especially those which form eutectics with AN, should be screened. It is desirable that future candidate fuels be less hygroscopic than MAN or QMAN. A fuel that forms a mixed crystal with AN should be sought.

Other methods for attaining an intimate mix or finer grain size should be considered. Examples of such methods are more rapid freezing, stirring during freezing, and coprilling or coprecipitation for use with TNT. (We successfully cocrystallized MAN/AN in 10-g quantities but were not successful in our limited effort to scale to kg quantities).

An effort should be made to determine if improved performance is due to chemistry (oxygen balance), to the AN particle size that results when a melt cosolidifies, or to some other factor.

More work on the methods for interpreting both small- and large-scale tests is needed. A less expensive large-scale test would be very desirable. A measurement of the equation of state of unreacted AN is needed to improve the interpretation of cylinder data.

VII. ACKNOWLEDGMENTS

(Picatinny Arsenal). The BKW calculations were performed by Charles L. Mader (LASL Group T-4). Group WX-2 (R. N. Rogers, M. J. Urizar, and H. H. Cady) prepared the small-scale samples and conducted the thermal and impact studies. Group WX-3 (A. Popolato, H. L. Flaugh, and L. E. Hatler) prepared the large-scale samples and performed analytic and coprecipitation studies. Experiments to measure performance were conducted by Group M-3.

VIII. REFERENCES

1. Henry Eyring, Richard E. Powell, George H. Duffy, and Ransom P. Parlin, Chem. Rev. 45, 69 (1949).

2. J. W. Kury, H. C. Hornig, E. L. Lee, J. L. McDonnel, D. L. Ornellas, M. Finger, F. M. Strange, and M. L. Wilkins, "Metal Acceleration by Chemical Explosives," Fourth Symposium (International) on Detonation, White Oak, Maryland, October 12-15, 1965.

3. J. Hershkowitz and J. Rigdon, "Evaluation of a Modified Cylinder Test of Metal Acceleration by Nonideal Explosives Containing Ammonium Nitrate," Picatinny Arsenal Technical Report 4611 (1974).

4. A. Popolato, A. W. Campbell, L. W. Hantel, H. R. Lewis, P. G. Salgado, and B. G. Craig, "Properties of Amatex/20," Los Alamos Scientific Laboratory Report LA-5516-MS (1974).

5. M. Finger, H. C. Hornig, E. L. Lee, J. W. Kury, "Metal Acceleration by Composite Explosives," Fifth Symposium (International) on Detonation, Pasadena, California, August 1970.

6. Charles L. Mader, "An Equation of State for Nonideal Explosives," Los Alamos Scientific Laboratory Report LA-5864 (1975).

7. J. Hershkowitz and I. Akst, "A New Approach to Improving the Performance of Non-Ideal Explosives Containing Ammonium Nitrate," Picatinny Arsenal Technical Report 4789 (1975).

8. J. B. Ramsay, B. G. Craig, H. L. Flaugh, T. Rivera, M. Schwartz, H. R. Lewis, and A. Popolato, "Feasibility of Using Amatex in Air Force Submunitions, "Los Alamos Scientific Laboratory Report LA-5992-PR(February 1974).

9. L. C. Smith, "On Brisance and a Plate Denting Test for the Estimation of Detonation Pressure," Explosivstoffe 5, 106-110, 130-134 (1967).

10. E. L. Lee, H. C. Hornig, and J. W. Kury, "Adiabatic Expansion of High Explosive Detonation Products," UCRL-50422 (1968).

11. M. Cowperthwaite and W. H. Zwisler, "Tiger Computer Program Documentation," Stanford Research Institute Projects 1182, 1281, and 1397 (March 1974).

12. M. J. Urizar, Los Alamos Scientific Laboratory, private communication (1975).

13. Charles L. Mader, "Theoretical Estimates of the Detonation Velocity of Explosives Containing Inert Diluents," Australian Defense Scientific Service Technical Memorandum 29 (1969).

14. Brigitta M. Dobratz, "Properties of Chemical Explosives and Explosive Simulants," UCRL-51319, p. 8-2, 8-12 (1972).

15. Department of the Army and the Air Force, "Mil. Explosives," Department of the Army and the Air Force Manual TM9-1910/TO11A-1-34, p. 120 (1955).

16. E. W. Washburn, Editor, International Critical Tables, Vol. V., p. 179,(McGraw-Hill Book Co., New York, NY 1929).

17. A. Popolato, Editor, "Joint Services Explosive Program, Los Alamos Scientific Laboratory Report LA-5616-PR (1974).

18. W. C. McCrone, Jr., "Fusion Methods in Chemical Microscopy," pp. 94-100 and 142-180, Interscience Pub., Inc., New York, NY (1957).

19. R. N. Rogers, Thermochimica Acta 11, 222 (1975).

20. Taylor B. Joyner, Naval Weapons Center, personal communication (1975).

21. T. L. Jordan, "Smoothing and Multivariable Interpolations with Splines," Los Alamos Scientific Laboratory Report LA-3137 (1965).

Charge Preparation: After DTA tests showed that it was safe to make melts combining AN with MAN or QMAN, charges for the small-scale experiments were prepared in two ways. The procedure for charges identified in Table I as either MAN/AN melt or QMAN/AN melt was as follows. The specified weight percents of AN and either MAN or QMAN were blended and a melt prepared. The melts were solidified as 2- to 3-mm-thick sheets. The sheets were broken and ground with mortar and pestle to obtain a product that passed through a #80 American standard sieve and was retained on a #230 sieve. The screened material was blended with RDX as required. Charges were pressed to diameter and then machined to length. The MAN for these charges was synthesized by LASL.

The procedure for preparing small-scale charges identified as eutectic melt differed in that the MAN was procured from E. I. duPont de Nemours & Co., Inc., and that the powder was prepared as follows. The eutectic composition of MAN/AN was prepared as an aqueous solution. The water was evaporated in a vacuum oven, and the eutectic mixture was melted into layers approximately 6-mm thick and quickly solidified to minimize crystal growth. To obtain the desired MAN/AN composition and particle size, the eutectic mixture of MAN/AN was crushed in a jaw mill, mixed with prilled AN, and ground twice through a Model 5H Mikro Pulverizer hammer mill. At this stage the powder passed through a #80 sieve. All fines were retained. The ground MAN/AN mixture was dry blended with RDX to produce the desired mixtures. The charges were pressed (138 kPa or 20,000 psi) to diameter and machined to length. All of these operations were performed remotely.

We resorted to the latter procedure after it was discovered that the quantity of powder required for large-scale tests could not be prepared by the first procedure but could be by the second. Charges for the large-scale tests were prepared by the second method except that both diameter and length were machined (dry) to dimension. Analytical results for the two mixtures prepared by the second method are presented in Tables A-1 and A-2.

The small-scale charges of RDX, RDX/AN, RDX/MAN, and TNT were prepared by blending as required, pressing to diameter, and machining to length. Two sizes of AN were used to prepare the RDX/AN charges. The AN identified as standard in Table I was of a particle size and distribution similar to that used in the second procedure for preparing RDX/MAN/AN charges, and identical to that used to prepare large-scale charges of RDX/AN. Analytical results for large-scale RDX/AN charges are given in Table A-3.

The results of thermal and impact studies are given in Appendix B. A tabulation of the densities obtained for the three formulations tested in large-scale are given in Table A-4. Based on the accuracy with which the weight and volume were determined, the error in the density should not exceed $3 \times 10^{-3} Mg/m^3$.

No quantitative data were obtained on the hygroscopic properties of MAN and AN. However, a number of qualitative observations were made during the preparation of the two formulations containing MAN as one of the constituents. In general, formulations containing a mixture of MAN and AN are significantly more hygroscopic than AN. At relative humidities between 30 and 50%, moisture was absorbed by the RDX/MAN/AN mixtures. Because of this, precautions were taken to keep the mixtures dry. The explosives were kept in well sealed containers and were only exposed to atmospheric environment during the pressing, machining, gauging, and assembly operations.

Formulations containing mixtures of MAN and AN were more corrosive than the 40 RDX/60 AN formulation. A brief exposure, at a relative humidity of about 30%, to steel inspection and machining tools resulted in significant corrosion of the tools.

Raw Materials: RDX The RDX used met the requirements of MIL-R-398C for Type B, Class G. Results of acceptance tests are presented in Table A-5.

Ammonium Nitrate (AN) The AN used in this study was a commercial grade of prilled AN meeting the requirements specified in MIL-A-50460. It was obtained from Terra Chemicals International, Inc.

TABLE A-1

ACCEPTANCE ANALYSIS OF RDX/MAN/AN

LOT 75-22

Lot Size = 45.5 kg

Property	Analytical Result	Requirement
Composition (wt%)		
RDX, Type B, Class C, Lot SR-3957, MIL-R-398	40.0	40.0
AN per MIL-A-50460	30.0	30.0
MAN, Lot 106	29.7	30.0
Water[a]	0.3	0.0
Bulk Density (Mg/m^3)	1.07	–
Median particle diameter MAN/AN (μm)	≈100	–
Vacuum Thermal Stability (ml/g 48 h 120°C)	1.0	–
Impact Sensitivity (H_{50}, m)		
Type 12	0.68	–
Type 12B	1.18	–
DTA (°C)		
First endotherm	≈50	–
First exotherm	≈205	–

[a]This is only a measure of water at the time the sample was analyzed. Because of the hygroscopic nature of this material, the moisture content was probably higher at a later time.

TABLE A-2

ACCEPTANCE ANALYSIS OF RDX/MAN/AN

Lot 75-19

Lot Size - 59 kg

Property	Analytical Result	Nominal Requirement
Composition (wt%)		
RDX, Type B, Class C, Lot SR-3957	39.0	40.0
AN	44.0	45.0
MAN, lot 106	16.5	15.0
Water[a]	0.5	0.0
Median particle diameter MAN/AN (μm)	≈100	-
Vacuum Stability (ml/g 48 h 120°C)	1.08	-
Impact Sensitivity (H_{50}, m)		
Type 12	0.59	-
Type 12B	0.87	-
DTA (°C)		
First endotherm	≈50	-
First exotherm	≈205	-

_____

[a]This is only a measure of water at the time the sample was analyzed. Because of the hygroscopic nature of this material, the moisture content was probably higher at a later time.

TABLE A-3

ACCEPTANCE ANALYSIS OF 40 WT% RDX/60 WT% AN

Property	Analysis	Requirement
Composition (wt%)		
RDX	38.7	40.0
AN	61.3	60.0
Impact Sensitivity (H_{50}, m)		
Type 12	0.493	–
Type 12B	0.642	–
Vacuum Stability (ml/g 120°C 48 h)	0.2	–
Bulk Density (Mg/m^3)	0.95	–

AN Particle Size Distribution

Sieve Size	Sieve Opening (μm)	Wt% Retained
120	125	0.5
170	88	2.3
230	62	5.4
325	44	32.9

(Median particle size < 40 μm)

No problems were encountered in the preparation of this mixture

TABLE A-4

DENSITY OF SEGMENTS FOR CYLINDER TESTS

(102-mm diameter by 102-mm high)

Composition (wt%) 40 RDX/60 AN		Composition (wt%) 40 RDX/15 MAN/45 AN		Composition (wt%) 40 RDX/30 MAN/30 AN	
Piece No.	Density (Mg/m^3)	Piece No.	Density (Mg/m^3)	Piece No.	Density (Mg/m^3)
36245-1	1.716	36326-1	1.671	36328-2	1.633
2	1.719	2	1.668	3	1.636
3	1.719	3	1.662	5	1.634
4	1.718	5	1.673	6	1.630
5	1.720	8	1.674	7	1.631
6	1.720	9	1.671	8	1.627
7	1.722	10	1.666	9	1.630
8	1.721	11	1.674	10	1.631
11	1.720	12	1.675	11	1.630
12	1.716	13	1.676	12	1.630
13	1.722	14	1.678	13	1.631
14	1.723	15	1.674	14	1.630
15	1.721	16	1.678	16	1.632
16	1.717	17	1.673	17	1.632
17	1.720	18	1.675	18	1.630
18	1.721	19	1.669	19	1.629
19	1.720	20	1.667	20	1.630
20	1.720	21	1.670	22	1.630
Av	1.720		1.672		1.631
Theoretical Density[a]	1.758		1.702		1.650

[a]Based on the nominal composition.

TABLE A-5

ACCEPTANCE ANALYSIS FOR RDX

Manufacturer- Holston Defense Corporation

Lot SR-39-57

Property	Analysis	Requirement of MIL-R-398C
Composition (wt%)		
RDX	92.3	NR[a]
HMX	7.7	NR
Melting point (°C)	188	190
Acetone insoluble (wt%)	Trace	0.05

RDX Particle Size Distribution

Sieve Size	Sieve Opening (μm)	Analysis (wt% passing)	Requirement of MIL-R-398C (wt% passing)
80	177	99.7	90 $\pm$ 2
120	125	93.2	
170	88	68.8	46 $\pm$ 15
230	62	38.7	
325	44	23.3	

(Median particle size ≈75 μm)

[a] Not required.

Acceptance testing was performed in accordance with the procedures specified in MIL-A-50460, Amendment 1. Results are given in Table A-6.

Methyl Ammonium Nitrate (MAN) The MAN used to prepare large charges was procured from E. I. duPont de Nemours & Co., Inc. as a 76% aqueous solution (Lot 106). Results of acceptance tests are given in Table A-7.

Tetramethyl Ammonium Nitrate (QMAN) The QMAN was analytical grade procured from Eastman Kodak, Eastman Organic Chemicals Division. No acceptance analysis was performed.

TABLE A-6

ACCEPTANCE ANALYSIS OF PRILLED AN

Manufacturer - Terra Chemicals

Lot RQT-KX3-22425-01

Property	Analysis	Requirement of MIL-A-50460
Moisture (wt%)	0.09	0.15 max
Acidity as HNO_3 (wt%)	0.03[a]	0.02 max
Ammonium Chloride (wt%)	<0.02	0.02 max
Diammonium Phosphate (wt%)	0.14[a]	0.21 ± 0.04
Diammonium Sulfate (wt%)	<0.007[a]	0.007 to 0.014
Boric Acid (wt%)	0.07[a]	0.14 to 0.03
AN (wt%)	98.60	98.50 min
pH	5.50[a]	5.9 ± 0.2
Bulk Density (Mg/m^3)	0.90	0.80 min
Particle Density (Mg/m^3)	1.50	1.50 min

[a]These values are outside specification limits.

TABLE A-7

ACCEPTANCE ANALYSIS OF MAN

Manufacturer - duPont

Lot 106

Property	Analysis	Requirement
Composition (wt%)		
MAN	>99.0	99.0
Impact Sensitivity (H_{50}, m)		
Type 12	0.71	-
Type 12B	2.22	-
DTA (°C)		
First endotherm	≈80[a]	-
Melt endotherm	≈110	-
First exotherm	≈275[b]	-

[a]Solid-solid phase transition MAN II to MAN I.

[b]Decomposition of melt.

THERMAL AND IMPACT STUDIES OF THE SYSTEMS MAN/AN AND QMAN/AN

An abbreviated investigation of the systems MAN/AN and QMAN/AN was conducted using the techniques of differential scanning calorimetry (DSC), differential thermal analysis (DTA), and thermal microscopy.

DSC. The heat of fusion of MAN was determined to be 11.08 ± 0.05 cal/g and the heat of transformation of MAN_{II} to MAN_I was determined to be 24.51 ± 0.009 cal/g with the DSC. Similarly, the heat of fusion of the prilled AN_I used in the phase diagram study was 17.55 ± 0.07 cal/g. This value is significantly lower than the literature value of 18.23 cal/g[15], but no effort was made to determine the reason for the discrepancy. The heat of transformation of AN_{II} to AN_I was determined to be 13.10 ± 0.05 cal/g which is slightly larger than the literature value of 12.84 cal/g[16]. These heats were determined to provide a calculated check for the measured liquidus lines of the reported phase diagrams.

Thermal Microscopy. Thermal microscopy observations were restricted to the temperature range from room temperature ($23 \pm 3°C$) to 300°C -- the temperature range of our Mettler hot stage. Phase identifications were not confirmed by x-ray diffraction and hence are subject to some uncertainty. This is especially true of the transitions in the vicinity of 50°C in the AN/QMAN system.

The thermal microscopy of AN has been reported in detail[17] and the phase transitions in pure AN are well understood. The transition of AN_{IV} to AN_{III} depends on the past history of the sample and the amount of water present. The effect of MAN or QMAN on the slow AN_{IV}-AN_{III} transition was not studied, but it is unlikely that this transition temperature is affected because neither MAN nor QMAN appreciably alters the transition temperature of $A_{,V}$ to AN_{II}. However, QMAN does form a limited solid solution with AN_I, and possibly other AN polymorphs, because the temperature of the AN_{II} to AN_I transformation changes from 126°C to 124°C in the presence of excess QMAN. The equilibrium transition temperatures measured for AN are -19°C for AN_V-AN_{IV}, 32.5°C for AN_{IV} to AN_{III}, 54°C for AN_{IV} to AN_{II}, 84°C for AN_{III} to AN_{II}, and 126°C for AN_{II} to AN_I and 169°C for the melting point of AN.

Pure MAN has an observed solid-solid transformation from MAN_{II} to MAN_I at 78.2°C and a melting point of 110.0°C by thermal microscopy. MAN_I is isotropic and hence crystallizes in a cubic space group.

A fusion slide was prepared by conventional techniques[18] covering the entire composition range from pure AN to pure MAN. Examination of this slide as a function of temperature indicated that the system is a simple eutectic system with a eutectic melting temperature between AN_{III} and MAN_{II} of 57.2°C. The transition between the AN polymorphs did not show any significant variation with MAN concentration nor did the MAN transformation temperature depend on the AN concentration. This means that there is little if any solid solution formation in the system.

Three mixtures of known composition were studied and were used to determine the eutectic composition and position of the liquidus curves in the system. The composition of the mixtures and their liquidus temperatures are summarized in Table B-1.

Pure QMAN was not studied by thermal microscopy because transitions were not observed by DTA in the temperature range available to the microscope hot stage. However, a temperature-controlled hot plate was used to observe the decomposition of QMAN at temperatures above 300°C. Between 300°C and 350°C QMAN decomposed slowly with charring but did not show any visible molten phase. Above 350°C a molten phase forms that proceeds to dissolve the remaining crystalline QMAN and then decomposes rapidly to gaseous products. A pronounced odor of amines accompanies both decompositions. The molten phase that forms above 350°C does not form instantly when a powder of QMAN is sprinkled on the hot surface so this is not a case of true melting, but

TABLE B-1

COMPOSITIONS AND LIQUIDUS TEMPERATURES OF MIXTURES

System	Wt% AN	Mole% AN	Excess Phase	Liquidus Temp. (°C)
MAN/AN	25	28.14	MAN_{II}	64-68
MAN/AN	50	53.89	AN_{II}	86
MAN/AN	75	77.90	AN_{II}	120
QMAN/AN	80	87.12	AN_{I}	142-143
QMAN/AN	74.1	82.98	$QMAN_{I}$	137
QMAN/AN	66.7	77.28	$QMAN_{I}$	170-180
QMAN/AN	50	62.97	$QMAN_{I}$	>210

rather it is a case of crystals dissolving in their own decomposition products.

A conventional fusion slide of QMAN/AN system could not be prepared because of the high melting point of QMAN and the rapid decomposition of the mixed melts above 200°C. A fusion slide was prepared covering the composition range from 50 wt% QMAN to 100 wt% AN. The slide was prepared in the presence of a steep thermal gradient that pure AN (mp 169°C) could be melted as the second phase and mixed in a narrow zone with the QMAN/AN mixture containing a eutectic melting at 133°C. The AN transition temperatures as a function of QMAN concentration did not change except for the $AN_{II} \rightarrow AN_{I}$ transition which was lowered 2°C to 124°C. The QMAN/AN eutectic melting covered a broad temperature range but finished at 133°C. The broad temperature range suggests that the QMAN studied is relatively impure. No evidence supporting compound formation between QMAN and AN was observed. The lowering of the AN_{II} and AN_{I} transition temperature implies some solid solution of QMAN in AN or at least in AN_{I}.

Four mixtures of QMAN and AN with known composition were studied and were used to determine the eutectic composition and position of the liquidus curves in the system. The mixtures decomposed rapidly above 210°C and it was not possible to determine the position of the liquidus curves above that temperature experimentally. The compositions of the mixtures and their liquidus points are given in Table B-1.

DTA. The pure compounds and the same mixtures used in the thermal microscopy studies were also investigated by DTA. DTA curves are not useful for measuring liquidus temperatures, except for eutectics, but are particularly useful for detecting low-temperature transformations and decomposition temperatures. A decrease in the temperature at which exothermic decomposition occurs is normally considered evidence of incompatibility and such a decrease occurs in the QMAN/AN system. RDX is partially soluble in the QMAN/AN eutectic melt and this further lowers the onset of exothermic reaction in the ternary system. Selected DTA curves are shown in Fig. B-1 through Fig. B-17.

The DTA curve for pure AN (Fig. B-1) shows that only a small fraction of the AN is transformed to AN_{III} below 85°C. The noise in the curve between the melting endotherm and the decomposition exotherm is indicative of gas evolution by the sample.

The curves for pure MAN (Fig. B-2) show clearly the phase changes in MAN and the thermal decomposition that becomes rapid about 260°C. The curves obtained on the MAN/AN mixtures are dominated by the eutectic melting endotherm. The DTA curve of the RDX/MAN/AN ternary mixture (Fig. B-8) shows a broad endotherm at the normal eutectic temperature. Microscopic examination of this mixture does not show RDX solubility in the melt.

QMAN (Fig. B-10) shows a structured transition between -25° and 10°C. This is called a simple polymorphic transition, but it may in fact involve more than two polymorphs. No x-ray studies have been undertaken to resolve this issue. The decomposition of QMAN above 300°C is unusual in that
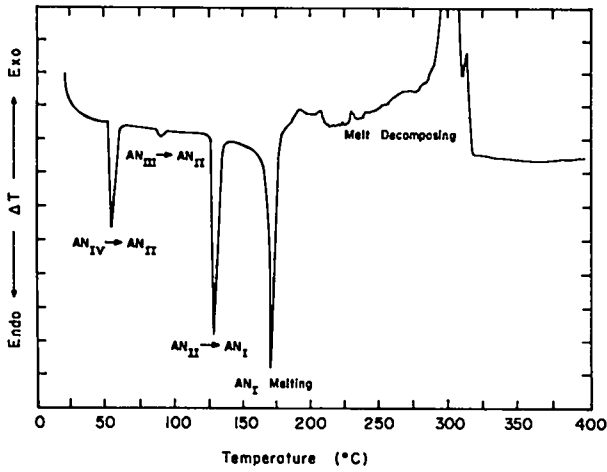
31

Fig. B-1. Curve for as-received AN (Batch 4067, medium ground). ΔT = 0.5°C/division, Rate = 20°C/min, Start T = 20°C.
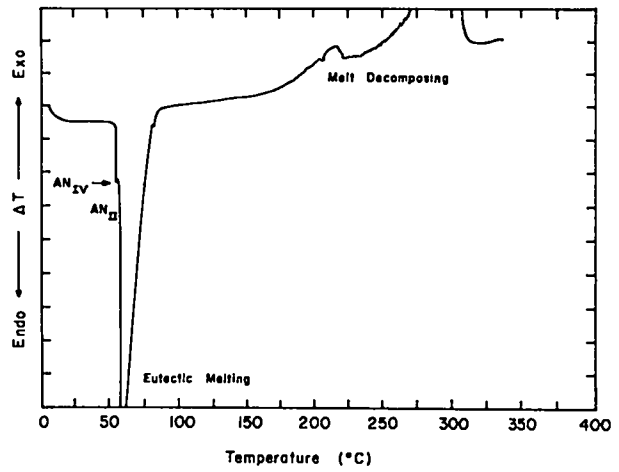
Fig. B-3. Curve for 75 MAN/25 AN, wt % (mixed powders). ΔT = 0.5°C/division, Rate = 20°C/min.
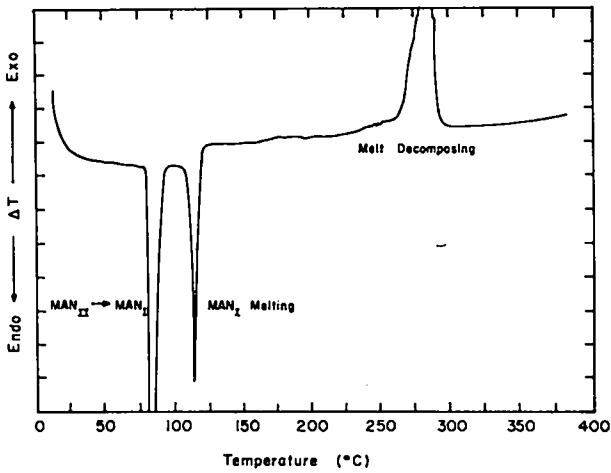
Fig. B-2. Curve for MAN produced by LASL. ΔT = 0.5°C/division, Rate = 20°C/min, Start T = 10°C.
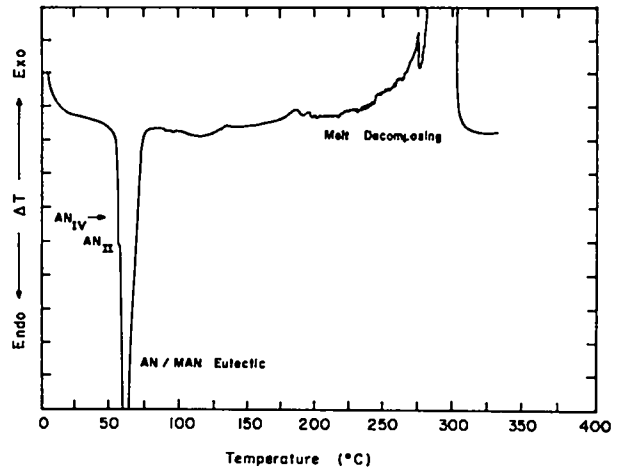
Fig. B-4. Curve for 50 MAN/50 AN, wt % (mixed powders). ΔT = 0.5°C/division, Rate = 20°C/min.

32
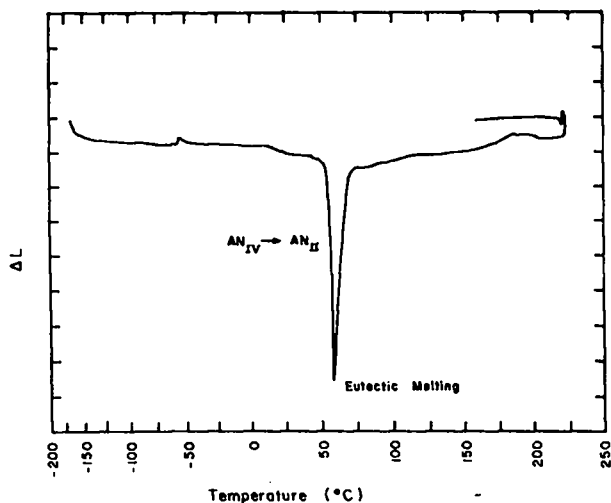
Fig. B-5. Curve for 50 MAN/50 AN, wt % (fused together at 150°C). Rate = 20°C/min, ΔL = 0.1°C/division.
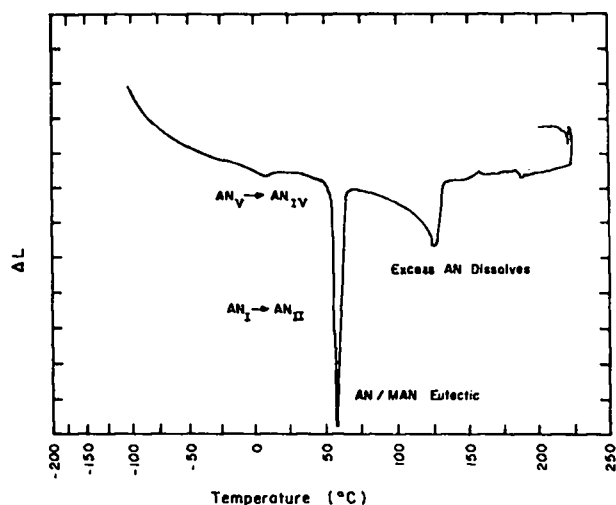
Fig. B-7. Curve for 25 MAN/75 AN, wt% (fused together at 150°C). ΔL = 0.5°C/division, Rate = 20°C/min.
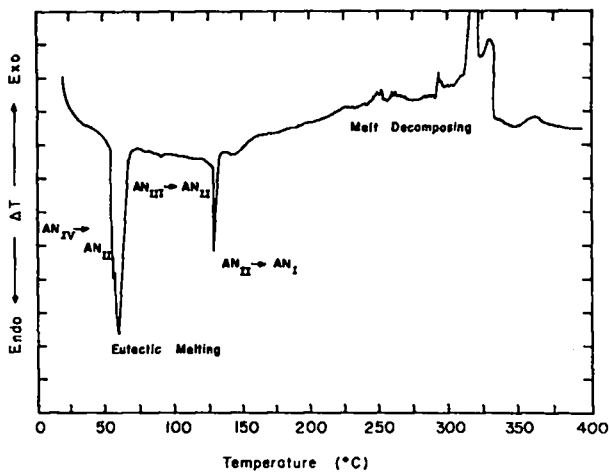
Fig. B-6. Curve for 25 MAN/75 AN, wt % (mixed powder). ΔT = 0.5°C/division, Rate = 20°C/min, Start T = 20°C.

Fig. B-8. Curve for 40 RDX/30 MAN/30 AN, wt % (mixed powders). ΔT = 0.5°C/division, Rate = 20°C/min, Start T = 0°C.

33
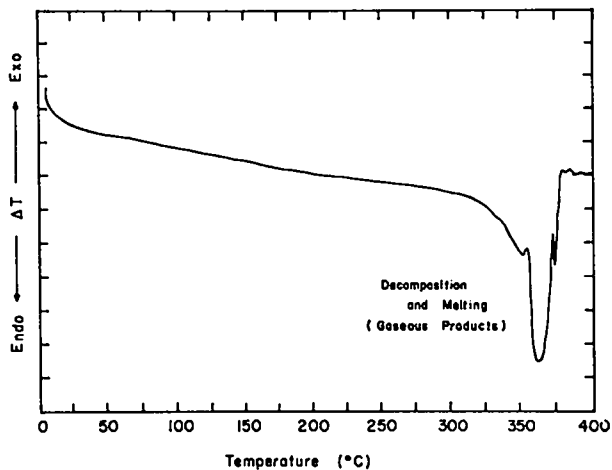
Fig. B-9. Curve for as-received QMAN (powder). ΔT = 0.5°C/division, Rate = 20°C/min.
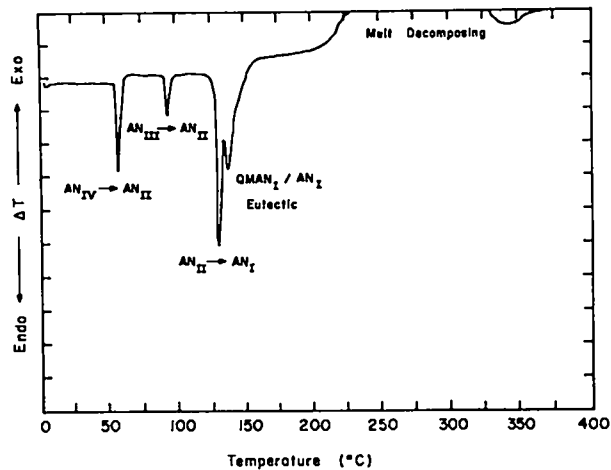
Fig. B-11. Curve for 20 QMAN/80 AN, wt % (mixed powders). ΔT = 0.5°C/division, Rate = 20°C/min, Start T = 0°C.
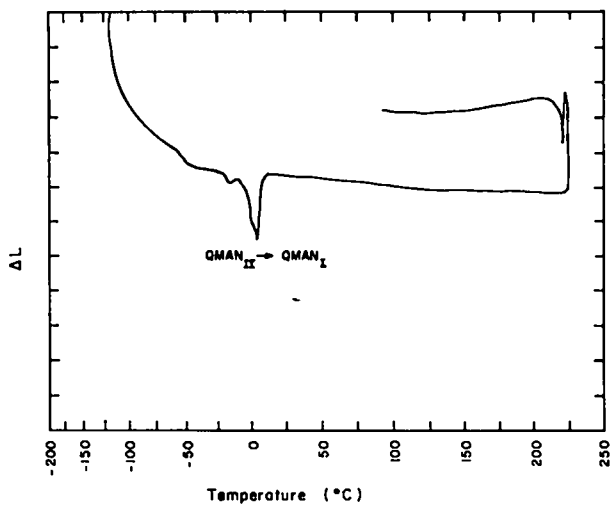
Fig. B-10. Curve for as-received QMAN (powder). ΔL = 0.5°C/division, Rate 20°C/min.
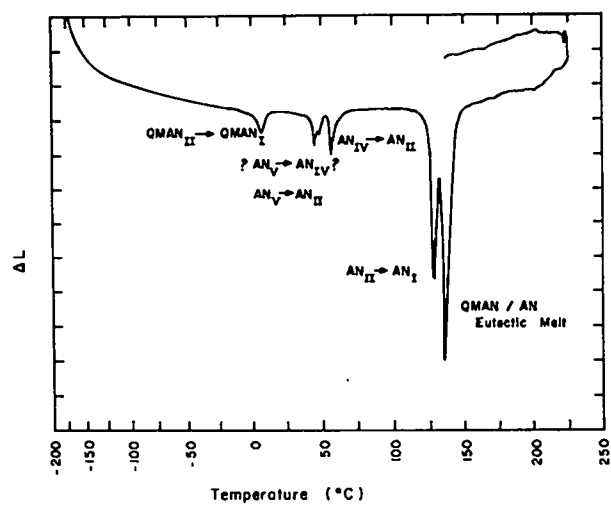
Fig. B-12. Curve for 20 QMAN/80 AN, wt % (fused together at 150°C). ΔL = 0.5°/division, Rate 20°C/min.

34
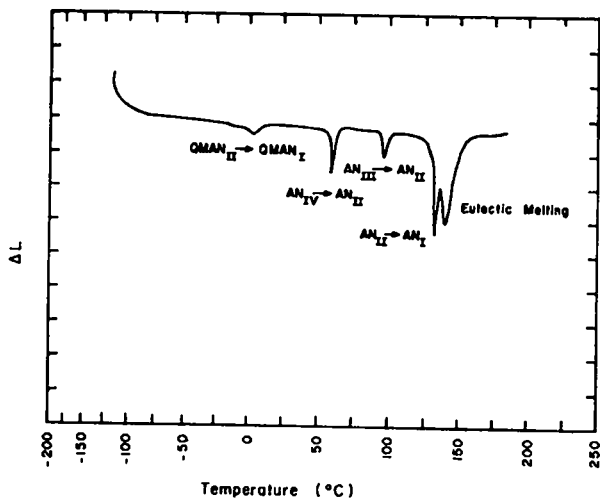
Fig. B-13. Curve for 26 QMAN/74 AN, wt % (mixed powders). ΔL = 1°C/division, Rate = 20°C/min.
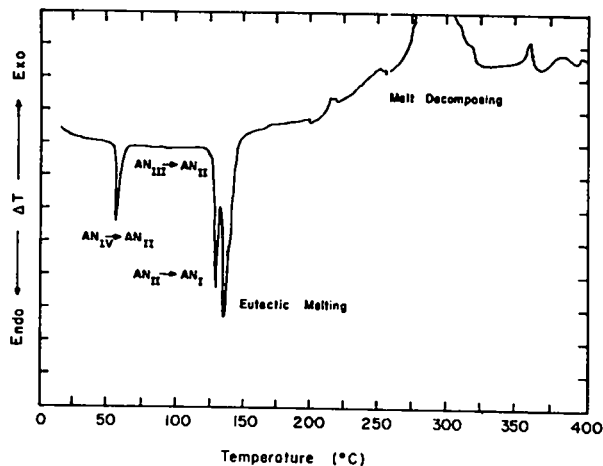
Fig. B-15. Curve for 50 QMAN/50 AN, wt % (mixed powders). ΔT = 0.5°C/division, Rate = 20°C/min, Start T = 0°C.
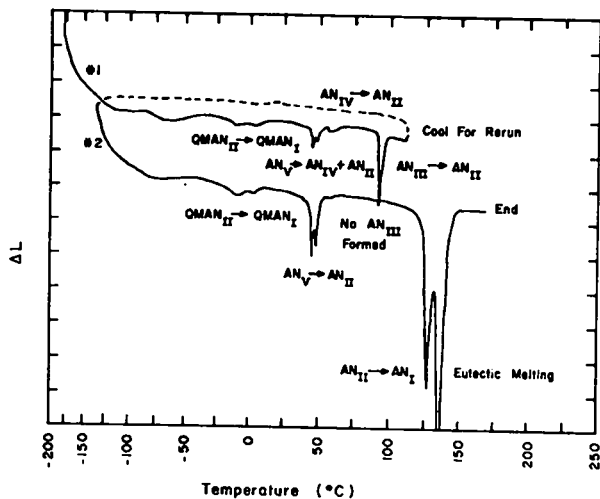
Fig. B-14. Curve for 26 QMAN/74 AN, wt % (fused together at 150°C). The sample was cooled with liquid nitrogen between cycles #1 and #2. ΔL = 0.5°C/division, Rate = 20°C/min (except cooling).
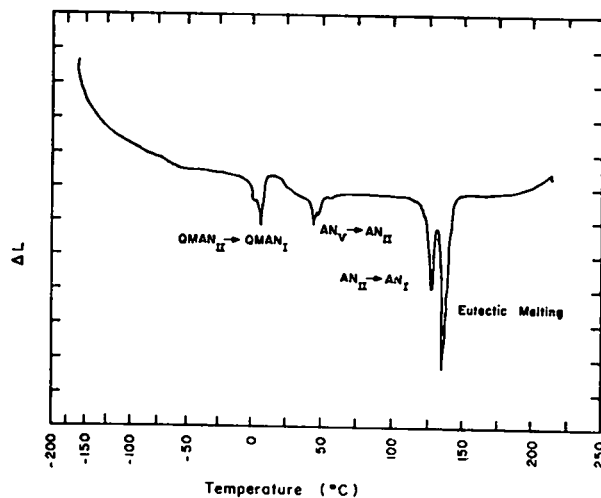
Fig. B-16. Curve for 50 QMAN/50 AN, wt% (fused together at 150°C). ΔL = 0.5°C/division, Rate 20°C/min.

35
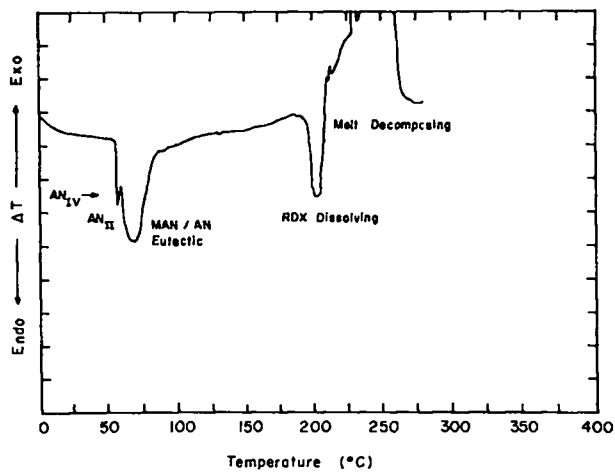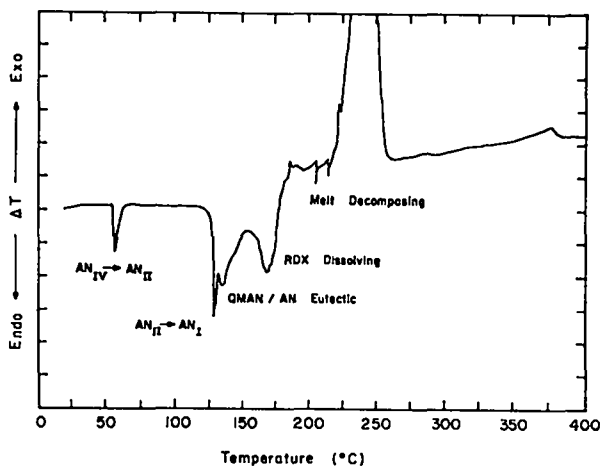
Fig. B-17. Curve for 40 RDX/30 QMAN/30 AN, wt %
(mixed powders). ΔT = 0.5°C/division,
Rate = 20°C/min, Start T = 0°C.

Fig. B-18. Phase diagram for the MAN/AN system.

the decomposition in both the solid state (300–
355°C) and in solution (355-375°C) is endothermic.

Pretreatment of the QMAN/AN mixtures by heating
to form a eutectic melt and then cooling with
liquid nitrogen causes a transformation of $QMAN_I$
to $QMAN_{II}$ (Fig. B-14) and a change in the AN phase
to form a polymorph (probably AN_V) that transforms
to AN_{II} between 40 and 50°C on warming. This
40-50°C endotherm is very reproducible and has two
peaks, but the reason for a double-peaked endo-
therm is unknown. In any case, these endotherms
involve transformations between metastable
polymorphs.

Phase Diagrams. The phase diagrams of the MAN/AN
and QMAN/AN systems are given in Figs. B-18 and
B-19. In comparing DTA curves with the phase
diagrams, it must be remembered that many of the
observed DTA transitions are between metastable
phases or occur at temperatures displaced from
their equilibirum positions. The dashed lines in
Fig. B-18 are calculated using Raoult's law and
the Clausius-Clapeyron equation,

$$\ln N = \frac{-\Delta H_f}{R} \left(\frac{1}{T} - \frac{1}{T_{mp}} \right);$$

the data are given in Table B-2. The calculation
ignores heat capacity and solid-solution effects --
either of which could account for the indicated
differences.

Dashed lines in the QMAN/AN phase diagram indicate
phase changes of uncertain position. The liquidus
points for $QMAN_I$ are used to estimate the melting
temperatures and heats of fusion of QMAN listed
in Table B-2.

Henkin. Henkin tests were performed to measure
explosion temperatures. The test as used has been
described by Rogers.[19] The data are summarized
in Table B-3 as temperature-time ranges and
calculated activation energies and pre-exponential
factors of the Arrhenius equation

$$k = Z \exp(-E/RT).$$

Impact. Drop-weight impact tests were performed
using pellets prepared as for the small-scale
tests. The data are summarized in Table B-4.
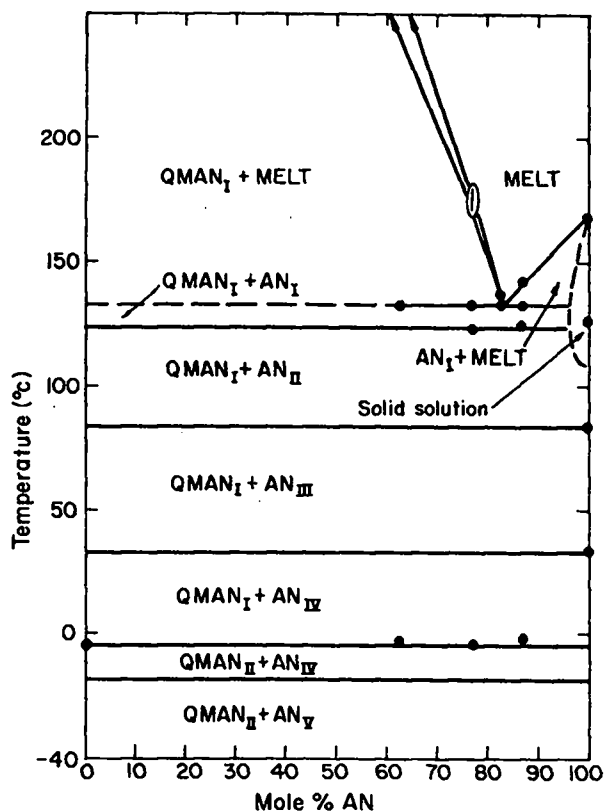
Fig. B-19. Phase diagram for the QMAN/AN system.

TABLE B-2

HEATS OF FUSION AND MELTING POINTS

Material	Source of Data	ΔH_f (cal/mole)	T_{mp} (°C)
AN_I	DSC	1405	169.6
AN_I	MAN/AN Diag.	1648	169.6
AN_I	QMAN/AN	1938	169.6
AN_{II}	DSC	2453	149.5
AN_{II}	MAN/AN	2854	149.5
AN_{III}	DSC + Ref. 20	2764	141.0
AN_{IV}	DSC + Ref. 20	3163	122.6
MAN_I	DSC	1042	110.0
MAN_{II}	DSC	3348	87.5
MAN_{II}	MAN/AN	3736	87.5
$QMAN_I$	QMAN/AN	2773-3157	582-482

Composition (wt%)	Temperature Range (°C)	Time Range (s)	Activation Energy (kcal/mole)	Pre-Exponential Factor (s^{-1})	Density (Mg/m^3)
100 RDX	215-217	≈200	47.1	2.02×10^{18}	1.806
100 AN	352	≈ 2	49.5	3.01×10^{16}	1.725
100 MAN	297	≈ 4	22.5	1.31×10^{8}	1.42
100 QMAN	350	≈ 10	78.2	1.85×10^{25}	1.25
40 RDX/60 AN	216	≈ 17	33.4[a]	3.5×10^{12}	1.75
40 RDX/60 MAN	249	≈ 4			1.525
20 RDX/80 MAN	254	≈ 4			1.455
40 RDX/15 MAN/45 AN	225	≈ 11			1.666
40 RDX/30 MAN/30 AN	216	≈ 18			1.622
40 RDX/45 MAN/15 AN	231	≈ 31			1.568
40 RDX/12 QMAN/48 AN	216	≈ 14			1.635
40 RDX/20 QMAN/40 AN	209	≈ 20			1.586
40 RDX/30 QMAN/30 AN	217	≈ 18			1.531

a   Reference 17.

Composition (wt %)	50% Height Type 12 (m)	Type 12B (m)	Theoretical Density (Mg/m^3)
100 AN	2E[a] of 10 at 3.20	No go at 3.20	1.725
100 MAN	0.574	2.62	1.42
100 QMAN	No go at 3.20	No go at 3.20	1.25
40 RDX/60 AN	0.419	0.781	1.758
40 RDX/60 MAN	0.603	0.710	1.554
20 RDX/80 MAN	0.689	1.25	1.484
40 RDX/15 MAN/45 AN	0.512	1.25	1.702
40 RDX/30 MAN/30 AN	0.517	1.11	1.650
40 RDX/45 MAN/15 AN	0.584	1.17	1.600
40 RDX/12 QMAN/48 AN	0.558	0.566	1.680
40 RDX/20 QMAN/40 AN	0.737	0.928	1.632
40 RDX/30 QMAN/30 AN	0.788	0.827	1.575
100 MAN (duPont)	0.710	2.22	1.42
50 MAN (duPont)/50 AN	0.819	1.80	
25 MAN (duPont)/75 AN	1.04	≈2.55	

a Explosions were observed because this test is run with a paper pad which serves as a fuel.

APPENDIX C

THE LEAST-SQUARES CUBIC SPLINE METHOD
TO FIT CYLINDER DATA

A common method of analyzing the cylinder test is to fit a seventh-order least-squares polynomial to the experimental radius-time data. The time derivative of this polynomial gives the desired velocity information. The effectiveness of this method was examined and it was found that the method results in errors that are probably small relative to the reproducibility error for the standard 25-mm-diameter cylinder test. However, a more sophisticated analysis is needed if one either improves the standard test (for example, by substituting helium for air as the surrounding medium to reduce refraction effects) or is concerned with details of the flow (such as wall reverberations). The least-squares cubic spline method was applied in order to provide a more sensitive numerical treatment and thus obtain as much information as possible from the experimental data. The general method has been described in a LASL report.[21]

Some of the advantages of this method are the following:

1. A set of splines allows greater local freedom in the fitting form than a globally fitted seventh-order polynomial.

2. Fitting of cubics allows the acceleration to change sign — which is what happens if the cylinder goes into tension.

3. The least-squares spline allows smoothing to be performed on the data.

4. Cubic splines join smoothly at their end points up to and including the second derivative.

The optimum number of cubics used for a fit is selected by allowing the number of cubics to increase until the standard deviation of the fit passes through a minimum. The standard deviation of a fit (σ) is given by

$$\sigma = \left\{ \sum_{i=1}^{NDAT} \left[R_i(exp) - R_i(cal) \right]^2 \middle/ [NDAT-p-1] \right\}^{1/2} , \quad (1)$$

where NDAT is the number of data points, R_i (exp) and R_i (cal) are respectively the ith experimental and calculated values of the radius and $p - 1$ is the number of cubics used in the fit. Figure C-1 shows a plot of σ as a function of the number of knots used in the spline fit; a knot is the position where two distinct cubics are joined. Note that on Fig. C-1, a large decrease in σ occurs at the 30-knot point. The peculiar structure in the σ curve, which shows numerous local maxima and minima, occurs because the various cubics were forced to extend over the equal increments of time. Another argument for using $\approx$30 cubics is the following. The standard deviation of data is thought to be approximately 7 μm. One would expect that when the fitting curve has sufficient flexibility, the variances of the fit and the experiments data would be approximately equal. Equation (1) can be used to determine p with this constraint on the two variances; it can be rewritten as

$$Q \, (data) \equiv \sum_{i}^{NDAT} \left[R_i(exp) - R_i(cal) \right]^2$$

$$= \sigma^2 \, (data) \, (NDAT-p-1). \quad (2)$$

When Eq. (2) is evaluated for σ (data) $= 7 \times 10^{-3}$ mm, one finds that Q (data) $\approx 2.31 \times 10^{-2}$. The same value results for Q when approximately 30 cubics are used. For 10-and 20-knot fits, there are large non-random bulges at early times — indicating that the structure at early times is not resolved by the fitting form.

Figure C-2 shows the velocities from a standard seventh-order polynomial fit and a 30-knot spline fit superimposed. One notes that the seventh-order fit is completely incapable of resolving the reverberation of the cylinder wall at early times. However, at late times a polynomial or a spline with fewer knots may be superior because of their greater power of smoothing.
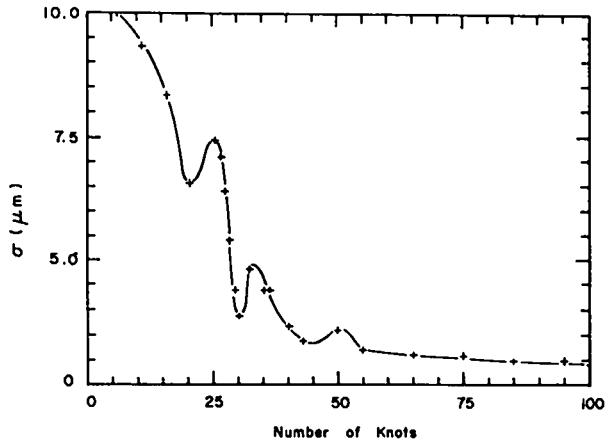
Fig. C-1. The standard deviation of the spline fits vs the number of knots. The structure in the curve is completely resolved between 25 and 30 knots.
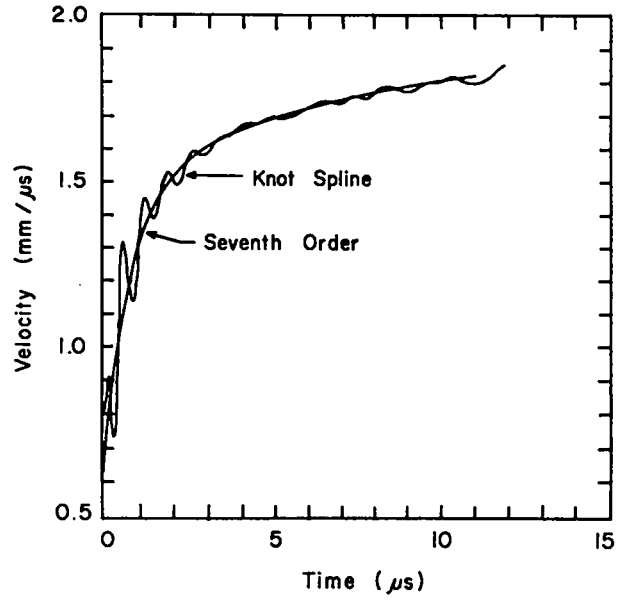
Fig. C-2. Superposition of the thirty-knot spline and seventh-order polynomial fits for a precision cylinder test.

APPENDIX D

DETAIL COMPARISON OF SEVENTH-ORDER POLYNOMIAL AND EIGHT-KNOT
SPLINE FITS TO CYLINDER EXPANSION DATA

Shot C-4506, 40 RDX/60 AN, 5.08-mm thick, 101.6-mm ID copper,
626 points used for fits; mass copper/volume of explosive [a]
$= 2.029$ Mg/m^3

R-Ro (mm)	7th-Order Polynomial		8-Knot Spline	
	t-to (µs)	Wall Velocity (mm/µs)	t-to (µs)	Wall Velocity (mm/µs)
6	5.664	1.371	5.672	1.382
8	7.068	1.474	7.063	1.488
10	8.388	1.553	8.374	1.559
12	9.650	1.615	9.636	1.610
14	10.869	1.664	10.860	1.656
16	12.056	1.705	12.053	1.698
18	13.217	1.740	13.218	1.734
20	14.357	1.769	14.361	1.766
22	15.479	1.796	15.484	1.794
24	16.585	1.819	16.591	1.819
26	17.678	1.840	17.684	1.840
28	18.759	1.860	18.765	1.860
30	19.830	1.878	19.835	1.879
32	20.890	1.895	20.894	1.897
34	21.941	1.911	21.944	1.914
36	22.983	1.926	22.984	1.929
38	24.017	1.941	24.017	1.944
40	25.044	1.954	25.043	1.960
42	26.064	1.966	26.061	1.969
44	27.078	1.979	27.074	1.981
46	28.086	1.989	28.081	1.991
48	29.089	1.999	29.083	2.000
50	30.087	2.008	30.081	2.008
52	31.081	2.017	31.073	2.016
54	32.071	2.024	32.066	2.022
56	33.058	2.030	33.053	2.027
58	34.041	2.036	34.039	2.032
60	35.023	2.040	35.023	2.036
62	36.002	2.044	36.004	2.040
64	36.979	2.048	36.983	2.044
66	37.955	2.050	37.961	2.048
68	38.930	2.053	38.937	2.051
70	39.904	2.055	39.911	2.054
72	40.877	2.056	40.884	2.058
74	41.850	2.058	41.855	2.060

DETAIL COMPARISON OF SEVENTH-ORDER POLYNOMIAL AND EIGHT-KNOT

SPLINE FITS TO CYLINDER EXPANSION DATA (Cont'd)

| R-Ro | 7th-Order Polynomial | | 8-Knot Spline | |
(mm)	t-to (μs)	Wall Velocity (mm/μs)	t-to (μs)	Wall Velocity (mm/μs)
76	42.821	2.059	42.825	2.063
78	43.792	2.061	43.794	2.066
80	44.762	2.062	44.762	2.068
82	45.731	2.064	45.729	2.069
84	46.700	2.067	46.695	2.071
86	47.667	2.069	47.661	2.072
88	48.633	2.072	48.626	2.073
90	49.598	2.074	49.591	2.073
92	50.561	2.077	50.555	2.073
94	51.523	2.080	51.520	2.074
96	52.484	2.082	52.484	2.075
98	53.444	2.084	53.448	2.077
100	54.404	2.085	54.410	2.079

---

a. The standard ratio is 2.0165 Mg/m^3 for this wall thickness.

Shot C-4509, 40 RDX/15 MAN/45 AN 5.08-mm thick, 101.6-mm ID copper
277 points used for fits; mass of copper/volume of explosive
$= 2.040$ Mg/m^3

R-Ro (mm)	7th-Order Polynomial			8-Knot Spline	
	t-to (μs)	Wall Velocity (mm/μs)		t-to (μs)	Wall Velocity (mm/μs)
6	5.498	1.352		5.489	1.362
8	6.908	1.478		6.886	1.474
10	8.220	1.568		8.210	1.548
12	9.468	1.632		9.474	1.618
14	10.675	1.680		10.687	1.679
16	11.852	1.718		11.861	1.726
18	13.005	1.751		13.008	1.759
20	14.137	1.783		14.135	1.788
22	15.249	1.814		15.245	1.817
24	16.342	1.845		16.337	1.846
26	17.417	1.874		17.413	1.872
28	18.477	1.900		18.475	1.894
30	19.524	1.920		19.525	1.913
32	20.561	1.935		20.565	1.930
34	21.592	1.945		21.598	1.947
36	22.618	1.953		22.621	1.964
38	23.640	1.965		23.635	1.978
40	24.651	1.993		24.644	1.986
42	25.642	2.050		25.651	1.988

Shot C-4512, 40 RDX/30 MAN/30 AN, 5.1-mm thick, 101.6-mm ID copper
588 points used for fit; mass of copper/volume of explosive
was not measured.

R-Ro (mm)	7th-Order Polynomial		8-Knot Spline	
	t-to (μs)	Wall Velocity (mm/μs)	t-to (μs)	Wall Velocity (mm/μs)
6	5.359	1.396	5.362	1.414
8	6.736	1.506	6.727	1.512
10	8.027	1.590	8.016	1.591
12	9.258	1.655	9.248	1.654
14	10.447	1.708	10.438	1.704
16	11.604	1.750	11.599	1.743
18	12.735	1.785	12.735	1.778
20	13.846	1.815	13.850	1.809
22	14.940	1.841	14.947	1.837
24	16.020	1.863	16.028	1.862
26	17.088	1.883	17.094	1.884
28	18.145	1.900	18.151	1.903
30	19.193	1.917	19.197	1.921
32	20.232	1.932	20.234	1.936
34	21.263	1.947	21.263	1.951
36	22.287	1.960	22.285	1.965
38	23.304	1.973	23.300	1.977
40	24.315	1.985	24.309	1.988
42	25.319	1.997	25.312	1.998
44	26.317	2.009	26.311	2.007
46	27.310	2.020	27.305	2.017
48	28.298	2.030	28.294	2.026
50	29.281	2.040	29.279	2.035
52	30.260	2.049	30.260	2.044
54	31.234	2.057	31.236	2.053
56	32.204	2.065	32.208	2.062
58	33.171	2.072	33.175	2.071
60	34.134	2.080	34.139	2.079
62	35.095	2.085	35.099	2.086
64	36.053	2.090	36.057	2.092
66	37.009	2.095	37.011	2.098
68	37.962	2.099	37.964	2.102
70	38.914	2.103	38.914	2.105
72	39.865	2.106	39.864	2.108
74	40.814	2.109	40.812	2.110
76	41.762	2.111	41.760	2.112
78	42.709	2.113	42.707	2.113
80	43.655	2.115	43.653	2.115
82	44.600	2.117	44.598	2.116

Shot C-4512 (Continued)

R-Ro (mm)	7th-Order Polynomial		8-Knot Spline	
	t-to (μs)	Wall Velocity (mm/μs)	t-to (μs)	Wall Velocity (mm/μs)
84	45.545	2.118	45.543	2.118
86	46.488	2.120	46.487	2.119
88	47.431	2.122	47.431	2.120
90	48.373	2.124	48.374	2.121
92	49.315	2.126	49.316	2.124
94	50.255	2.129	50.260	2.127
96	51.194	2.131	51.196	2.131
98	52.131	2.134	52.134	2.136
100	53.068	2.137	53.069	2.141

Shot C-4508, 40 RDX/60 AN, 10.2-mm thick, 101.6-mm ID copper
584 points used for fits; mass of copper/volume of explosive
was not measured

R-Ro (mm)	7th-Order Polynomial		8-Knot Spline	
	t-to (μs)	Wall Velocity (mm/μs)	t-to (μs)	Wall Velocity (mm/μs)
6	7.208	0.983	7.259	0.999
8	9.158	1.066	9.186	1.076
10	10.975	1.132	10.990	1.140
12	12.700	1.186	12.705	1.192
14	14.354	1.231	14.351	1.236
16	15.955	1.268	15.946	1.271
18	17.513	1.299	17.501	1.300
20	19.037	1.325	19.025	1.324
22	20.533	1.348	20.523	1.346
24	22.006	1.367	21.999	1.365
26	23.460	1.384	23.455	1.382
28	24.897	1.399	24.894	1.397
30	26.320	1.412	26.319	1.410
32	27.731	1.423	27.732	1.421
34	29.132	1.433	29.135	1.431
36	30.524	1.442	30.528	1.440
38	31.907	1.450	31.913	1.448
40	33.283	1.457	33.290	1.457
42	34.652	1.464	34.659	1.464
44	36.016	1.470	36.022	1.471
46	37.373	1.476	37.379	1.478

Shot C-4508 (Continued)

| R-Ro | 7th-Order Polynomial | | 8-Knot Spline | |
(mm)	t-to (μs)	Wall Velocity (mm/μs)	t-to (μs)	Wall Velocity (mm/μs)
48	38.725	1.482	38.730	1.483
50	40.073	1.487	40.075	1.489
52	41.415	1.492	41.416	1.494
54	42.753	1.497	42.752	1.499
56	44.087	1.502	44.085	1.503
58	45.417	1.506	45.413	1.507
60	46.743	1.510	46.738	1.511
62	48.066	1.514	48.060	1.515
64	49.385	1.518	49.379	1.518
66	50.701	1.522	50.696	1.520
68	52.014	1.525	52.010	1.523
70	53.324	1.528	53.322	1.526
72	54.632	1.531	54.631	1.529
74	55.937	1.533	55.938	1.532
76	57.241	1.535	57.243	1.534
78	58.542	1.537	58.545	1.536
80	59.843	1.539	59.846	1.539
82	61.141	1.541	61.145	1.541
84	62.439	1.542	62.443	1.542
86	63.736	1.543	63.739	1.544
88	65.032	1.544	65.034	1.545
90	66.327	1.545	66.328	1.546
92	67.622	1.545	67.622	1.546
94	68.916	1.546	68.915	1.547
96	70.209	1.548	70.208	1.548
98	71.500	1.549	71.499	1.549
100	72.791	1.551	72.789	1.551

Shot C-4510, 40 RDX/15 MAN/45 AN, 10.2-mm thick, 101.6-mm ID copper
522 points used for fits, mass copper/volume of explosive [a]
= 4.049 Mg/m^3

R-Ro (mm)	7th-Order Polynomial		8-Knot Spline	
	t-to (μs)	Wall Velocity (mm/μs)	t-to (μs)	Wall Velocity (mm/μs)
6	6.892	0.998	---	------
8	8.817	1.073	---	------
10	10.626	1.136	10.615	1.073
12	12.347	1.188	12.396	1.169
14	14.000	1.233	14.054	1.241
16	15.595	1.271	15.632	1.292
18	17.148	1.304	17.157	1.328
20	18.665	1.333	18.650	1.348
22	20.151	1.357	20.126	1.364
24	21.613	1.379	21.584	1.379
26	23.054	1.397	23.027	1.393
28	24.477	1.414	24.456	1.407
30	25.884	1.428	25.871	1.420
32	27.278	1.441	27.272	1.434
34	28.660	1.453	28.662	1.446
36	30.032	1.463	30.039	1.458
38	31.394	1.472	31.406	1.469
40	32.749	1.481	32.763	1.479
42	34.096	1.489	34.111	1.488
44	35.436	1.496	35.451	1.497
46	36.771	1.503	36.783	1.505
48	38.099	1.509	38.109	1.513
50	39.421	1.515	39.428	1.520
52	40.739	1.521	40.741	1.526
54	42.051	1.527	42.049	1.532
56	43.358	1.532	43.353	1.536
58	44.661	1.538	44.653	1.541
60	45.960	1.543	45.949	1.545
62	47.254	1.548	47.243	1.548
64	48.544	1.552	48.534	1.551
66	49.831	1.557	49.822	1.554
68	51.114	1.561	51.108	1.558
70	52.394	1.565	52.390	1.561
72	53.670	1.568	53.670	1.565
74	54.944	1.572	54.947	1.568
76	56.216	1.574	46.221	1.572
78	57.485	1.577	57.491	1.576
80	58.752	1.579	58.759	1.579
82	60.018	1.581	60.025	1.582

Shot C-4510 (Continued)

R-Ro (mm)	7th-Order Polynomial		8-Knot Spline	
	t-to (μs)	Wall Velocity (mm/μs)	t-to (μs)	Wall Velocity (mm/μs)
84	61.283	1.582	61.289	1.584
86	62.546	1.583	62.551	1.586
88	63.809	1.584	63.812	1.587
90	65.071	1.585	65.072	1.588
92	66.332	1.586	66.331	1.589
94	67.593	1.587	67.590	1.589
96	68.853	1.588	68.848	1.590
98	70.112	1.590	70.106	1.590
100	71.369	1.592	71.364	1.590

a   The standard ratio is 4.0331 Mg/m^3 for this wall thickness.

Shot C-4511, 40 RDX/30 MAN/30 AN, 10.2-mm thick, 101.6-mm ID copper
543 points used for fits, mass copper/volume of explosive

$= 4.052 \ Mg/m^3$

R-Ro (mm)	7th-Order Polynomial		8-Knot Spline	
	t-to (μs)	Wall Velocity (mm/μs)	t-to (μs)	Wall Velocity (mm/μs)
6	6.765	1.019	---	-----
8	8.650	1.101	8.692	1.117
10	10.412	1.167	10.432	1.180
12	12.086	1.221	12.090	1.232
14	13.693	1.266	13.685	1.274
16	15.249	1.304	15.233	1.309
18	16.764	1.336	16.745	1.336
20	18.246	1.362	18.229	1.360
22	19.702	1.385	19.688	1.381
24	21.135	1.405	21.126	1.400
26	22.550	1.422	22.546	1.417
28	23.949	1.437	23.949	1.433
30	25.335	1.449	25.339	1.446
32	26.709	1.461	26.716	1.458
34	28.073	1.471	28.082	1.469
36	29.429	1.480	29.438	1.480
38	30.776	1.488	30.786	1.489
40	32.117	1.496	32.125	1.498
42	33.450	1.503	33.457	1.506
44	34.778	1.510	34.782	1.513
46	36.099	1.517	36.101	1.519
48	37.415	1.523	37.415	1.525

| R-Ro | 7th-Order Polynomial | | 8-Knot Spline | |
(mm)	t-to (μs)	Wall Velocity (mm/μs)	t-to (μs)	Wall Velocity (mm/μs)
50	38.725	1.529	38.723	1.531
52	40.031	1.535	40.027	1.537
54	41.331	1.541	41.326	1.542
56	42.626	1.547	42.621	1.547
58	43.917	1.552	43.911	1.552
60	45.203	1.558	45.198	1.557
62	46.486	1.563	46.481	1.561
64	47.763	1.567	47.760	1.566
66	49.038	1.572	49.035	1.570
68	50.308	1.576	50.307	1.574
70	51.576	1.580	51.577	1.578
72	52.840	1.583	52.842	1.582
74	54.102	1.587	54.106	1.585
76	55.361	1.589	55.366	1.589
78	56.619	1.591	56.623	1.592
80	57.875	1.593	57.879	1.594
82	59.130	1.595	59.133	1.596
84	60.383	1.596	60.385	1.598
86	61.636	1.597	61.637	1.599
88	62.888	1.598	62.888	1.599
90	64.140	1.599	64.138	1.599
92	65.390	1.600	65.389	1.600
94	66.640	1.601	66.638	1.601
96	67.889	1.603	67.887	1.603
98	69.135	1.606	69.133	1.606
100	70.379	1.610	70.377	1.610